University of Oulu
Department of Chemistry
P.O. Box 3000
FIN-90014 University of Oulu
FINLAND

THEORETICAL INVESTIGATION IN THE STRUCTURAL PROPERTIES, BONDING AND REACTIVITY OF SOME CHALCOGEN COMPOUNDS

TEEMU TAKALUOMA

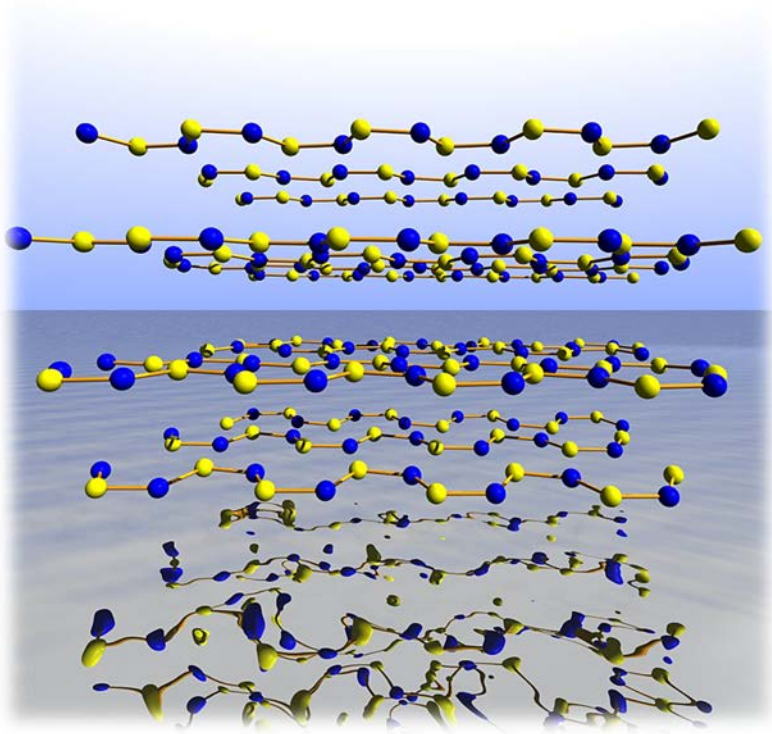

REPORT SERIES IN CHEMISTRY
Report No. 89 (2013)

OULUN YLIOPISTON KEMIAN LAITOKSEN

RAPORTTISARJA

UNIVERSITY OF OULU, REPORT SERIES IN CHEMISTRY

REPORT No. 89 (2013)

(Received August, 2013)

Theoretical investigation in the structural properties, bonding, and reactivity of some chalcogen compounds

TEEMU TAKALUOMA

Academic Dissertation to be presented with the assent of the Doctoral Training Committee of Technology and Natural Sciences of the University of Oulu for public discussion in OP-Pohjola-sali (Auditorium L6), Linnanmaa, on the 13th of September, 2013, at 12 o'clock noon.

DEPARTMENT OF CHEMISTRY

UNIVERSITY OF OULU GRADUATE SCHOOL

UNIVERSITY OF OULU

LINNANMAA

FI-90014

OULUN YLIOPISTO

FINLAND

Editor

Professor Osmo Hormi

Department of Chemistry

P. O. Box 3000

90014 University of Oulu

Finland

ISBN 978-952-62-0186-3 (Paperback)

ISBN 978-952-62-0193-1 (PDF)

ISSN 0358-528X (Printed)

OULUN KOPIOKESKUS / MULTIPRINT

OULU 2013

Abstract

In this thesis the bonding, structural properties, and chemical reaction pathways have been investigated for several different types of chalcogen-containing molecules. The work encompasses sulfur nitride polymers, metal complexes of selenium diimides, organic disulfide nitrosonium adducts and chalcogenidoborate anions. Novel work on the explanation of the polymerization pathways of the disulfur dinitride ring presents the first example of a molecular dynamics simulation study on a topochemical reaction in the field of inorganic chemistry. Structural and bonding analysis of dinuclear copper(I) and silver(I) selenium diimides has been carried out to investigate the d^{10}-d^{10} closed-shell interactions with the Atoms in Molecules theory. Molecular orbital analysis of organic disulfide nitrosonium adducts show a clear and chemically intuitive reaction mechanism. Stabilities of yet unknown adducts have also been considered. The possibility to prepare hitherto unknown hybrid chalcogenidoborates has been explored by theoretical methods. The trends in their structures and bonding have also been discussed.

Acknowledgements

This present work was carried out in the Department of Chemistry at the University of Oulu during the years 2006-2013.

I wish to express my deepest gratitude and thanks to Prof. Risto Laitinen for his supervision of this work. His guidance and support has carried through the whole dissertation. I would also like to express my thanks to him for the introduction to the fascinating world of main group chemistry.

Professor Kari Laasonen provided fundamental help with the theoretical work concerning molecular dynamics and for that I am deeply grateful for him. I would also like to thank Dr. Tom Bajorek for his help in the beginning of my work. He paved the foundation from which I could build up my own expertise.

I am very grateful to all of my co-authors for their contributions. The Department of Chemistry and especially our research group has provided a friendly and innovative working environment and I sincerely acknowledge all of my colleagues and the whole staff in the Department for their support. The pre-examiners of this dissertation, Prof. Pipsa Hirva and Dr. Heikki Tuononen, are also warmly acknowledged for their comments and suggestions.

The financial support from the Inorganic Materials Chemistry Graduate Program (ETMKO) and the Academy of Finland is gratefully acknowledged. I would also like to thank the Finnish CSC – IT Center for Science for their extensive provision of computer resources and the help from their highly proficient staff.

Finally, I would like to express my gratitude to my family and especially my parents for their endless support during my studies. I would also like to thank my beloved wife Esther, and our daughters Helena and Matilda, for their support and love.

Oulu, August 2013

Teemu Takaluoma

List of original articles

This dissertation is based on the following original papers, which are referred to in the text by Roman numerals.

I. Takaluoma, T. T.; Laasonen, K.; Laitinen, R. S. *Inorg. Chem.* **2013***, 52*, 4648-4657.

II. Risto, M.; Takaluoma, T. T.; Bajorek, T.; Oilunkaniemi, R.; Laitinen, R. S.; Chivers, T. *Inorg. Chem.* **2009***, 48*, 6271-6279.

III. Mueller, B.; Takaluoma, T. T.; Laitinen, R. S.; Seppelt, K. *Eur. J. Inorg. Chem.* **2011***,* 4970-4977.

IV. Takaluoma, T.; Säkkinen, T.; Bajorek, T.; Laitinen, R. S.; Krebs, B.; Conrad, H.; Conrad, O. *J. Mol. Struct.* (THEOCHEM) **2007,** *821*, 1-8.

The author of this thesis is the principal contributor for writing the original manuscript of paper I. In papers II and III all the theoretical work was carried out by the author. The author is also the principal contributor for writing the theoretical parts of the original manuscripts of papers II and III. On paper IV majority of the theoretical work was carried out by the author and he was also the principal contributor for writing the paper. Dr. Tom Bajorek performed the ELF analysis in paper IV and acted as a supervisor in papers II and IV. Undergraduate student Tero Säkkinen performed part of the computations in paper IV supervised by the author of this thesis.

Contents

1 Introduction

The global impact of main group chemistry has been significant. Discoveries like the Haber process and Ziegler-Natta catalysts, both very important for industrial processes, were recognized by Nobel prizes in 1918 and 1963, respectively.[1] Manufacturing methods for silicone polymers is another very high impact area of main group chemistry. Understanding of the chemical bonding has also been strongly driven by main group chemistry. Pauling and Gillespie have done much in explaining the structural properties in chemistry. Pauling's book *The Nature of the Chemical Bond*[2] is one of the most influential books written about chemical bonding. His work on chemical resonance, valence bond theory and concepts of electronegativity are seminal.[2-3] Gillespie's theory of Valence Shell Electron Pair Repulsion (VSEPR) continues to be powerful and intuitive tool in qualitative prediction of structural properties.[4] The better understanding of the relationship between the chemical bonding and molecular structure continues to be the driving force of research in main group chemistry. The heavier main group elements have been likened to transition metal compounds with similarities in bonding, coordination and reactivity.[5] New discoveries, like the multiple bonded main group species such as R—Si≡Si—R continue to challenge the current theories on chemical bonding.[6]

Inorganic main group chemistry has seen renaissance during the recent decades with strong prospects in the future for novel applications in the field of superconductors, battery technology, finger printing, photovoltaic cells, light-emitting diodes and many others.[7-17] Novel practical applications rising from the basic research in main group chemistry

continue to be strong. During the year 2012 and in early 2013 already 117 patents have been granted concerning chalcogen containing materials.[18] During the same time period work concerning “sulfur nitrides” or “poly thiazyls” has resulted in 30 patents.

CdTe photovoltaic (PV) cells are globally important with a market share of around 10% with strong growth.[19] The most common CdTe thin-film solar cells are composed of a p-type CdTe absorber layer and an n-type CdS window. The record conversion efficiency for the CdTe PV cell is 16.5%. $Cu(In,Ga)Se_2$ and $Cu(In,Al)Se_2$ cell materials are also very attractive thin-film applications with the conversion efficiencies of almost 20% and 17.5%, respectively.

New multiband PV materials based on $Pb_{0.2}Eu_{0.8}E$ (E=O, S, Se, Te) have been proposed as an improvement over traditional Si- or GaAs-based cells.[13] The europium 4f electronic states are between its 6s5d states and the p-states of the chalcogen atom. This allows for absorption of photons on multiple energy ranges without a need for doping as the multiband properties arise naturally from europium chalcogenides. Solar cells manufactured from these materials can result in a significantly better conversion rate than cells made from conventional semiconductor materials.

Poly sulfur nitride has been used in several patents concerning new secondary *i.e.* rechargeable batteries.[11] Other possible new applications for this polymer are in novel piezo-electric materials[9] or in flexible materials for the solar cell production.[2] Poly chalcogen nitrides and chalcogen-containing semiconducting materials have significant and very promising

uses in practical applications needing new durable, cost-efficient, and high-performing materials. Poly sulfur nitride has also seen promising use as an imaging agent in forensics.[10,17] Quite unexpectedly, disulfur dinitride was observed to polymerize preferentially on various impurities or imperfections on different surfaces. A metal surface washed clean by an explosion still has minute corrosion left from a finger print. The interaction of disulfur dinitride with this corrosion signature brings out the image of the finger print. Ink diffused through envelope, finger prints on cloth or on pottery can all be visualized with the preferential polymerization of the disulfur dinitride. Most, if not all, conventional forensics imaging techniques are inadequate with these materials, especially if the finger print deposit itself has been physically removed prior to the analysis.

This thesis explores the chemical bonding and reactions of several types of chalcogen-containing molecules using quantum chemical methods. Density functional theory (DFT) and Atoms in Molecules (AIM) analysis have extensively been employed as the main theoretical tools. Power of molecular dynamics (MD) solid state simulations is illustrated in the study of the polymerization pathways of disulfur dinitride. The research is a part of the long-term goal towards the synthesis of selenium-containing chalcogen nitride polymers, which may have enhanced electrical properties compared to the known sulfur nitride polymer.

Paper I presents the first solid-state MD simulation of inorganic topochemical reaction. The archetypal topochemical polymerization of the S_2N_2 has been extensively investigated. The connection of the

polymerization pathways and the reaction activation to the disorder in the resulting polymer has been explored.

Paper II concentrates on the synthesis and theoretical analysis of dinuclear copper and silver complexes containing selenium diimide ligands. These compounds exhibit d^{10}-d^{10} closed-shell metallophilic interactions. The nature of the interaction has been explored with electron density analysis based on AIM at theoretical levels ranging from HF and DFT to post-HF, using in particular the 2nd order Møller–Plesset perturbation theory (MP2).

Paper III describes the stability trends of the cations containing NO^+ and organic disulfides. Molecular orbital (MO) and AIM analysis have been applied to provide the description for the adduct formations.

Paper IV reports the structural and stability trends of sulfur- and selenium-containing borate anions BE_3^{3-}, $B_2E_4^{2-}$, $B_2E_5^{2-}$ and $B_3E_6^{3-}$. Extensive bonding analysis has been performed and the replacement of sulfur by selenium has been analyzed. Paper IV is currently the only research article in existence were the still experimentally elusive hybrid chalcogenidoborate anions have been investigated.

2 Computational details

2.1 High-pressure molecule dynamics[I]

The high pressure MD simulations were performed with the CP2K[20] program using the QUICKSTEP[21] implementation. RevPBE[22-23] density functional with Grimme's[24-25] D3 empirical dispersion correction was used in the simulations. QUICKSTEP uses dual-basis representation: atom centered Gaussian basis in combination with planewaves.[21] In the MD simulations molecular optimized short range DZVP[26] (DZVP-MOLOPT-SR) with GTH[27-28] pseudopotentials was used for the Gaussian-part and an energy cutoff of 350 Ry was used for the planewaves. The DZVP-MOLOPT-SR is constructed from the DZVP-MOLOPT basis set by removing two highest-exponent primitives. All methods have been used as implemented in CP2K.

The dynamics part used an NVT-type ensemble. A canonical sampling through velocity rescaling (CSVR)[29] thermostat was used with a timestep of 100.0 fs. The simulations were done using the cell-optimization (cell_opt) method in CP2K. Each simulation cell change was evaluated from 50 MD steps with 4.0 fs timestep. The MD-runs were used to compute the stress tensors for the cell optimization. To simulate the high pressure compression, a pressure tensor was applied to the cell optimization stress tensor. Temperature in the simulations was either 300 K or 600 K. The high-pressure simulations were started from super cell versions (2x2x1 and 4x4x2) of an experimentally determined β-S_2N_2 [30] structure.

The selection of proper method for the optimization of the wavefunction is important when quantum chemical computations are combined with molecular dynamics.[31-32] Non-optimal choice can result either in very slow converge or even in divergence of the wavefunction optimization. Optimal parameters are highly dependent on the chemical system under investigation. Significant improvement in the energy convergence and the computer time required for energy convergence steps can be achieved with some preliminary benchmarking.

For the simulation of the S_2N_2 polymerization, the combination of a direct inversion in the iterative subspace (DIIS) minimization with a polynomial orbital transformation based on refinement expansion (OT/IR) with a full single inverse type preconditioner, as implemented in the CP2K program, was found to be optimal choice.[31] The efficiency of the preconditioner and the minimizer may change at different pressure regions. The generally more expensive and robust full all type preconditioner may become more efficient as the electronic states become more complicated at high pressures. The DIIS may also have convergence problems at high pressure states in which case conjugate gradients (CG) method may be superior. Intermitted benchmarking during long simulations is recommended especially after significant changes have occurred in the electronic structure of the model system.

2.2 Gas-phase and implicit solvation computations[II-IV]

The copper- and silver complexes were computed with Turbomole 5.10 [33] and Gaussian 03 [34] and Gaussian 09 [35] programs.[II] Computations of the chalcogenidoborate anions were also performed with Gaussian 03 program.[IV] The disulfide adducts were computed with Gaussian 09 program.[III] Expect for the MO orbital analysis, the disulfide computations included implicit solvation correction based on the CPCM[36] model using acetonitrile as solvent (T = 298.15 K, 101.325 kPa). Atoms in Molecules (AIM) analysis[37-38] has been done with Aimpac[39,I], AIM2000 [40,II] and AIMAll[41,III] programs. Papers III and IV have made use of the electron delocalization index (DI) method.[42] The DI method computes an estimate of the bond order by calculating the average number of electrons delocalized (shared) between two atomic centers.

Paper II involved computations using PBE[22,43], RIMP2 and RICC2[44-49] with def-TZVP[50-56], def2-TZVP[50-56], def2-TZVPP[50-56], and def2-QZVPP[51-57] basis sets. Computations in paper III were done at the M06L[58] level involving the def2-TZVPP basis set. Basis sets were obtained from the Basis Set Exchange (BSE) database.[59-60] The computations in paper IV were performed with the PBE0 [22,43,61] density functional and with the MP2 electron correlation theory[62] using the 6-311+G(2d) basis sets.[63-65]

3 Polymerization of disulfur dinitride

3.1 Background

Poly sulfur nitride $(SN)_x$ was discovered by Burt in 1910 as then unknown sulfur nitride.[66] While heating yellow tetrasulfur tetranitride (S_4N_4) through silver gauze at 200-300˚C, he observed the formation of a blue film with the evolution of nitrogen gas and a build-up of silver sulfide on the gauze. The blue film appeared to have bronze-colored metallic luster in reflected light.

Modern interest for polymeric sulfur nitride, which is obtained as layered or fibrous crystals, was sparked in 1970 with the discovery of its superconductive properties.[7-8,67] It is an anisotropic conductor and becomes a superconductor at the very low temperature of 0.26±0.03 K. Depending on purity, the room temperature conductivity along the polymer strands is 1–4 x 10^5 S/m which becomes two magnitudes larger at 4.2 K.[9,68] Perpendicular to the strands the conductivity is ca. 10^3 S/m at room temperature. For comparison doped polyacetylenes have room temperature conductivities in range of 1–6 x 10^4 S/m,[69] whereas metallic copper has a conductivity of 6 x 10^7 S/m.[70]

Several synthetic routes have been devised for the polymer. The classical route, based on Burt's original synthesis, is still the best source for high-purity crystalline polymer.[9] The reaction is presumed to happen in two steps.[71] First the vaporous S_4N_4 reacts with silver gauge to produce silver sulfide and nitrogen gas (Eq. 1). Silver sulfide will then catalyze the cleavage of S_4N_4 to S_2N_2 (Eq. 2). Thus formed S_2N_2 will then undergo

topochemical polymerization to $(SN)_x$. The polymerization is a slow process. Depending on the reaction conditions, it will take anything from few hours to weeks or even longer to reach completion. Several modifications of this classical synthetic path have been devised as has been reviewed in literature.[9,71] Generally higher temperatures (>280˚C) produce a purer product avoiding any S_4N_4 from passing through, although unreacted S_4N_4 is easily isolated from S_2N_2. Pressure also affects the synthesis and purity.

$$S_4N_4 + 8Ag \xrightarrow{140\text{-}305\ ^\circ C} 4Ag_2S + 2N_2 \quad (1)$$

$$S_4N_4 \xrightarrow{Ag_2S} S_2N_2 \quad (2)$$

The explosive nature of both the starting material S_4N_4 and the intermediate S_2N_2 has prompted the search for alternate synthetic routes.[9] Electrolysis of $[S_5N_5]^+$ produces thin films of $(SN)_x$.[72] Powdered $(SN)_x$ can be produced in a reaction between $(NSCl)_3$ and Me_3SiN_3 which avoids many of the problems in the classical route, since it does not involve S_2N_2 or S_4N_4.[73] Another, safer synthesis is the method by Roesky *et al.*[74] where S_4N_4 is reacted with $S_2N_2{\cdot}2AlCl_3$ to produce S_2N_2. The intermediate $S_2N_2{\cdot}2AlCl_3$ is obtained from reaction between S_4N_4 and $AlCl_3$. Compared to the direct pyrolysis of S_4N_4 shown in Eq. 1 this reaction proceeds at 80 ˚C. Several other methods are also known for the preparation of $(SN)_x$.[9]

Crystals of $(SN)_x$ show twinning, disorder and/or lack of long-range coherency, as exemplified in Table 1.[30,75-78] The structure determined by Boudelle[77] shows a significant distortion from the planarity, which may

well be a result from the disorder in atomic positions or from lack of coherency of the chains in the crystal structure. The other structures also show varying degree of disorder, defects and polymorphism. No good-quality ordered crystal structure has been determined for $(SN)_x$. This has been discussed below.

Table 1. Defects and disorder in the crystals of $(SN)_x$

Authors	R-factor	Defects and disorders
Boudeulle[a] (1975)	0.19[f]	Deviation from planarity, N-S-N-S 154°
Cohen *et al*[b] (1976)	0.111	73% occupancy of main chain + 3 x 9% occupancy of sulfur atoms from minor chains, twinning
Baughman *et al*[c] (1977)		twinning, structural disorder
Heger *et al*[d] (1978)	0.109[g]	defect ratio of 1:9 for detect to ordinary sites, defect sites are not unique and are occupied in equal ratio by sulfur and nitrogen
Müller *et al*[e] (1997)	0.135	90% main polymer, 10% other polymorph, no atom locations determined

[a] Ref. 77, [b] Ref. 30, [c] Ref. 75, [d] Ref. 78, [e] Ref. 76, [f] electron diffraction, [g] neutron diffraction

The electronic structure of the S_2N_2 ring is complicated and has been extensively studied. The nature of the bonding in the ring continues to be under debate. Tuononen *et al.*[79-80] have estimated, based on analysis of CI-vectors of CAS(22,16) wavefunction, that the 6π-electron sulfur nitride ring has the singlet diradical character of 6%, concentrated on the nitrogen atoms. Lewis-type valence bond analysis for the same wavefunction gives a weight of 34% for a structure with the singlet diradical character on nitrogen atoms and 14% weight for a structure where the singlet diradical character is concentrated on sulfur atoms.[79] Some of the earlier work has

placed the diradical nature on the sulfur atoms. Jung *et al*.[81] disagree with the assessment of diradicals in S_2N_2 and instead have proposed an aromatic 2π-electron system**.** Braida *et al.*[82] has proposed, based on valence-bond computations, that the singlet diradicals account for nearly 50% of the CAS(22,16) wavefunction, where the main weight is placed on singlet diradicals located on the nitrogen atoms.

The current research agrees with the concept that the singlet diradicals are concentrated on the nitrogen atoms, with some contribution also present in the sulfur atoms.

3.2 The Mechanism for the polymerization of S_2N_2

The mechanism for the topochemical polymerization of $(SN)_x$ from S_2N_2 has been investigated in several occasions since the first crystal structure measurements. The mechanisms have been reviewed by Labes *et al*.[71] and more recently by Banister and Gorrell.[9] First detailed theoretical studies on the mechanism were performed by Baughman *et al*.[75,83-85] Three pathways were envisaged, all of which resulted in the polymer formation along the *a* axis. Each was based on the principle of least motion, which was characterized by the root-mean-square displacement (RSMD):

1. *a* axis translation (single-bond cleavage)
2. *b* axis translation (single-bond cleavage, out-of-plane opening)
3. 2_1 axis propagation (formation from SN-radicals)

The first two involve a single-bond cleavage of each S_2N_2 ring, while the third involves the intermediate formation of SN-radicals.[83] The pathway 1 was found to have the smallest RSMD of 0.48 Å, while the pathway 2 resulted in displacements of 1.20 Å. The pathway 3 shows RMSD values of 1.25-1.40, with the smaller value corresponding to the undetected all-*trans* polymer chain. Powder diffraction studies by Müller *et al.*[86] also identified the *a* axis direction as the main mode for polymerization.

Mawhinney and Goddard[86] have proposed quite a different pathway. In their theoretical investigations concerning the singlet- and triplet potential energy surfaces of a single S_2N_2 ring in the gas-phase, they have proposed that the main reaction pathway would proceed through out-of-plane ring opening,[86] corresponding to the pathway 2 considered by Baughman *et al.*[83] Involvement of acyclic $(SN)_2$ and SN radical intermediates has also been proposed based on the mass spectroscopic decomposition studies.[87]

3.3 Molecular crystals in high pressure

Application of high pressure on molecular liquids and solids has a significant effect on the unit cell volume, electronic properties and reactivity.[88] Molecular materials are highly compressible and even a relatively mild pressures of 1 GPa can result in a 25% reduction of the volume. At high pressures, the intermolecular distances shorten and the repulsive part of the intermolecular interactions becomes comparable to the intramolecular interactions. In these conditions, the system can become thermodynamically unstable resulting in changes in the molecular

packing or in initiation of chemical reactions. The application of pressure can significantly affect the reaction kinetics.[89] Alternative reaction paths may appear and the reactions can either be accelerated or inhibited kinetically. The solid-state environment and especially highly pressurized states impose significant geometrical constraints for the mobility of possible reactive species.[90] On the basis of the topochemical principle, the solid state reaction mechanisms usually follow the pathways with least amount of atomic or molecular displacements.[91]

Energy level distribution in solid materials generally broadens with increasing pressure.[90] At the extreme case, the HOMO-LUMO gap can vanish resulting in a continuum. The polymerization of ethylene shows how the high pressure can alter the potential energy surfaces leading to reactions. At low pressures (< 5.4 GPa) ethylene polymerizes as a linear polymer, but at higher pressures the polymerization can propagate in two directions resulting in a highly branched polymer.

Theoretical modeling of solid-state chemical reactions in high pressure is still a relatively new field, which is not surprising considering the computational requirements to achieve large enough a simulation cell and to be able to calculate accurately the electronic states at high pressures. One closely related field that has become very active during the last few years is the theoretical modeling of pressure-induced phase transitions using MD simulations.

Two archetypal reactions have been extensively studied both experimentally and theoretically; the high-pressure reactivity of solid benzene and the high-pressure polymerization of solid acetylene. In a high-pressure study of the reactivity of crystalline benzene, a clear connection has been made between the high-pressure reaction pathway and the excited electronic states.[92] Two-photon absorption of benzene at 16 GPa compression results in an identical reaction to the photoexitation-free compression at 25 GPa. The high-pressure and photo-exitation reactions are qualitatively analogous in this case. In another experimental study, crystalline benzene was studied under 23 GPa and 540K.[93] Theoretical AIMD simulations to model this reaction at this pressure required 1500 K to overcome the limited time-scale (the simulation lasted 300 fs before reaction activation) of the simulation.[94] No reaction in these simulations were observed at the experimental temperature of 540 K even in pressures reaching up to 150 GPa.

Acetylene is considered to be one of the benchmark systems for the high-pressure polymerization reactions.[88] Polymerization of acetylene is usually achieved by use of the catalysts. However, the application of high pressure on crystalline acetylene can also lead to polymerization. It is initiated at the external pressure of 4.2 GPa and proceeds to near completion when pressure is increased to ~14 GPa.[95] The polymerization of acetylene has been modeled using constant-pressure MD.[96] In the course of the simulation, the cell containing 16 C_2H_2 molecules was first compressed at a pressure of 9 GPa in RT. The polymerization was initialized with a rapid increase of temperature to 400 K and pressure to 25 GPa. The process was very fast (a fraction of a picosecond). Another simulation with a more

gradual and steadier pressure increase on a unit cell consisting of 32 C_2H_2 molecules also resulted in the polymerization at 25 GPa. With the larger simulation cell the polymerization was more disordered, propagating in several directions and resulting in shorter fragments. Furthermore, two of the 32 molecules failed to polymerize. The differences were attributed to the speed of compression, and also to the small simulation cell that can favor polymeric structures. Seeding the system with a triplet-exciton acetylene molecule allowed the polymerization to be initiated already at the pressure of 9 GPa.

3.4 Molecular dynamics simulations of S_2N_2 at high pressure[I]

The polymerization of acetylene and the reactivity of benzene in high pressure simulations show that chemical reactions can be modeled in the solid state. High compression and temperature are necessary to increase the reaction rates. In the modeling of the polymerization of S_2N_2, similar concepts were applied to improve the reaction rates.[I] Simulations were performed on two model systems; a 2x2x1 supercell (221) and a 4x4x2 supercell (442) of the experimental β-S_2N_2.[30] Two different kinds of main simulations were performed; the fast compression of the 442 and the slow compression of the same cell. Preliminary testing was done with the smaller 221 cell. The 221 simulations qualitatively agree with the more robust 442 simulations.

In the 442 simulations, the pressure was incrementally increased from 0 GPa up to 50-57 GPa. In the fast compression method the pressure was increased in a step-wise fashion after the simulation has lasted for 4-8 ps. In the last pressure increase to 57 GPa, the reaction was observed immediately suggesting that the system is well past the activation barriers and the last pressure increase acted as a rapid shock to the system. Thus it was not surprising that significant and persistent side reactions were observed.

The slow compression was accomplished with significantly longer simulation periods between pressure increase steps.[I] The final three pressure steps (at 600K), 35 GPa, 45 GPa and 50 GPa, were simulated for 34.0, 30.0 and 70.0 ps, respectively. The first reaction was initiated after 58 ps simulation at the 50 GPa compression. The energy profile with the pressure and temperature details of the slow simulation is presented in Figure 1.

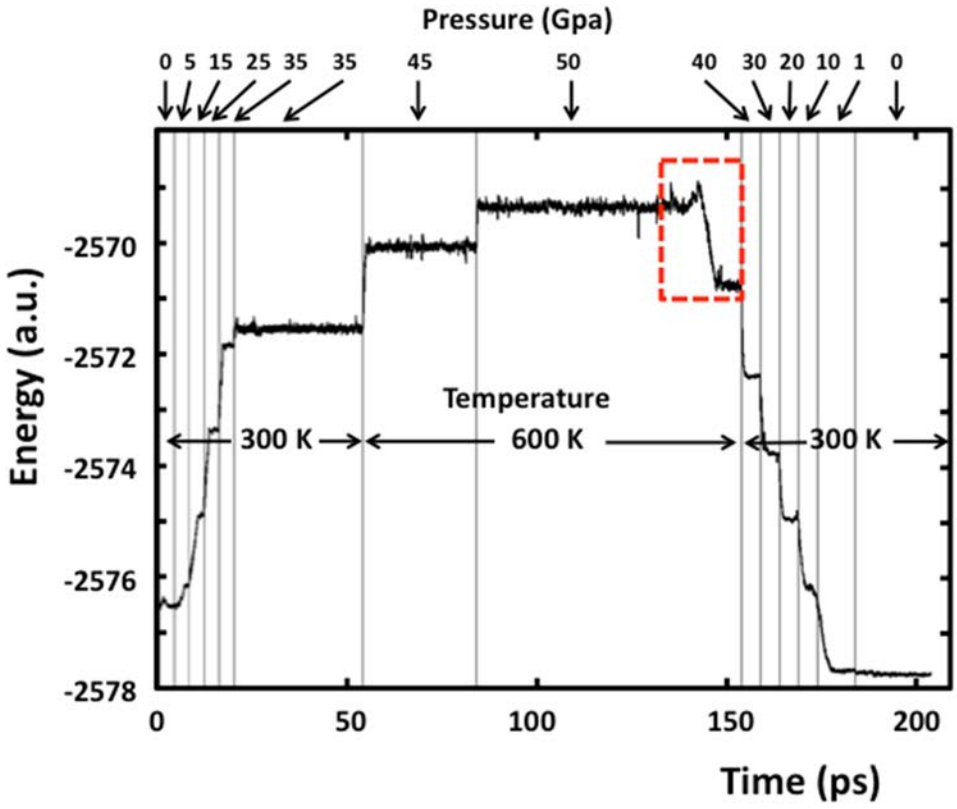

Figure 1. Energy variance during the topochemical simulation of S_2N_2. The pressure and temperature during given simulation times is shown. The rectangular area (t=140-152 ps) indicates the main reaction activation and polymerization part of the simulation.[I]
"Reprinted with permission from *Inorg. Chem*. **2013**, *52*, 4648-4657. Copyright 2013 American Chemical Society."

Before the reaction, the simulation remained very stable with no qualitative changes in the packing or in the shape of the simulation cell other than the decrease in the simulation cell volume because of the compression.[I] The S_2N_2 structure maintained its solid state cohesion well. The reaction stage was fast with the whole system being fully polymerized in five picoseconds. After the reaction, the pressure was lowered in steps

(see Fig. 1). Some minor packing changes were observed, when the pressure was lowered. Although the pressure in the simulations is high, it is still within a reasonable range. The superconductivity of $(SN)_x$ has been studied at up to 40 GPa compression without any observed decomposition of the polymer.[97]

The polymerization is activated with a single-bond cleavage, which rapidly propagates along row of rings in the direction of *a* axis.[I] Several side reactions are observed both in *b* and *c* axes directions. The interactions are short-lived and the oligomers revert back to the S_2N_2 rings before the onset of stable polymer chains along *a* axis. Figure 2 shows the energy profile of the reaction phase with three snap shots from the simulation.

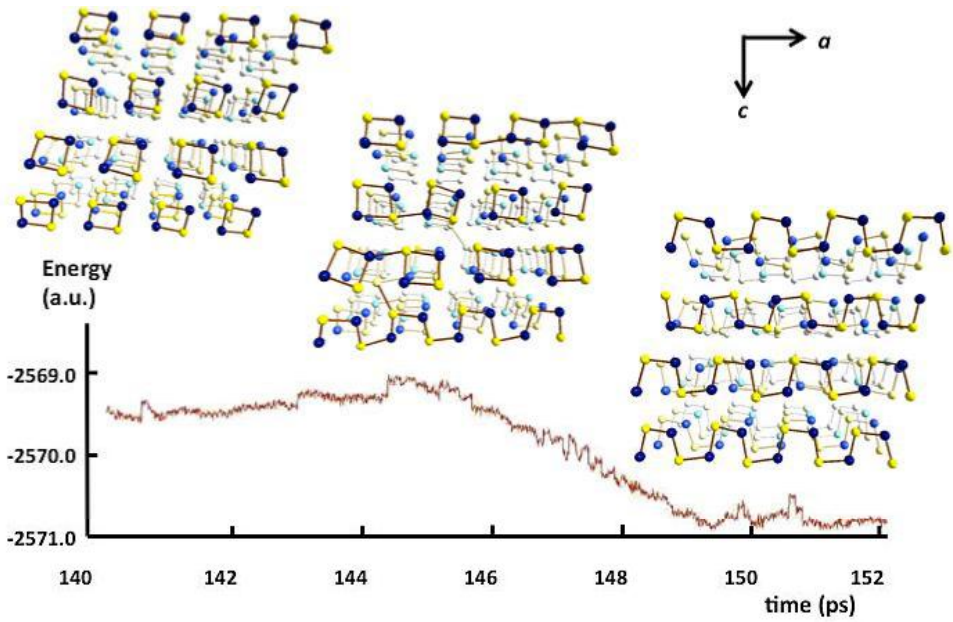

Figure 2. The energy profile of the polymerization of S_2N_2 at 50GPa and 600K. The simulation time corresponds to the reaction phase. (See the red rectangular area in Fig. 1.) Sulfur atoms are indicated by yellow spheres and nitrogen atoms by blue spheres.[I] "Reprinted with permission from *Inorg. Chem*. **2013**, *52*, 4648-4657. Copyright 2013 American Chemical Society."

While S_2N_2 and fully polymerized $(SN)_x$ do not show an electron paramagnetic resonance signal, it has been detected during the polymerization.[71,98] In the high-pressure MD simulations of $(SN)_x$, the main simulations were performed with restricted DFT formalism modeling the reaction at the singlet state.[I] Few tests were also performed with the triplet state wavefunction. The polymerization was generally observed in a slightly lower pressure or temperature, but otherwise no other qualitative differences were detected compared to the singlet state simulations. Both the singlet- and triplet-state reactions propagated along the row of ring molecules and are nearly instantaneous after the ring opening. In many

simulations short-lived side reactions were observed which, at least within the theoretical model, would seem to be a more likely source for the ESR signal than the highly reactive and very short-lived S_2N_2 chains, which are formed because of the ring opening.

Figure 3 illustrates the packing change from S_2N_2 to $(SN)_x$.[I] It has been proposed that while the polymerization occurs through the single-bond cleavage, the packing change from the herringbone structure of S_2N_2 to the layered packing of $(SN)_x$ would occur prior to the bond cleavage.[76] This is not likely, since there is no energetic reason for the rings to undergo 45˚ rotations with a simultaneous shear, as has been proposed.[I] If the packing of the rings would adopt a planar geometry prior to polymerization, both the *a*-axis and *c*-axis directions would be equally likely for the polymerization. Instead of the observed 90% polymer formation along *a* axis and 10% other polymorph(s)[76] the system would have at least two polymorphs close to equal statistical distribution.[I]

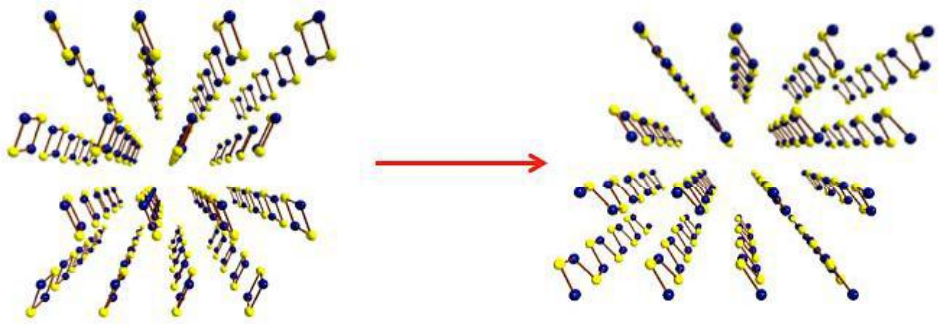

Figure 3. Packing differences of S_2N_2 (left) and $(SN)_x$ right. Sulfur atoms are indicated with yellow spheres and nitrogen atoms by blue spheres.[I] "Reprinted with permission from *Inorg. Chem.* **2013**, *52*, 4648-4657. Copyright 2013 American Chemical Society."

The solid state MD simulations did not show any indication for the change in the packing prior to the polymerization.[I] Instead, the packing in the simulation cell changes towards the end of the polymerization process.

In summary, the modeling of reactions in high pressures require long simulation times, and the activation is not expected to occur fast (under 5-10 ps) after the temperature or pressure in the system have been changed. If the change in the physical conditions is large, it can act as a shock in the system, which can push the unrelaxed system over higher energy barriers than in the more tempered model. Very fast activation, especially if reactions occur in less than a picosecond, can lead to the overemphasis of the side reactions.

3.5 Selenium-containing analogs of disulfur dinitride

One of the main targets in the research of heavier chalcogen-nitrogen compounds is the preparation of $(SN)_x$ analogues. It is expected that selenium- or tellurium-containing chalcogen nitride polymers might well have enhanced electrical properties such as higher transition temperatures to superconductivity.

Although the synthesis of $(SN)_x$ by thermolytic cleavage of S_4N_4 *via* the intermediate S_2N_2 is well known, similar reaction does not occur in case of Se_4N_4.[7-8] It is very unstable and its vapor pressure is very low. Instead Se_4N_4 undergoes decomposition to N_2 and elemental selenium. Because of this, other sources for Se_2N_2 have been under investigation.

In the series EE'N_2 (E,E'=S, Se, Te) only the S_2N_2 has so far been characterized in solid state. However, several complexes, in which Se_2N_2 acts as a bridging ligand coordinating from the two nitrogen atoms, have been prepared: $[Pd_2(\mu\text{-}Se_2N_2)X_6]^{2-}$ (X=Cl,Br)[99-100] and $[Al_2(\mu\text{-}Se_2N_2)Br_6]^{2-}$.[101] These could act as sources for Se_2N_2. In a recent study by Kelly *et al.*[102] $[Bu_4N]_2[Pd_2(\mu\text{-}Se_2N_2)Br_6]$ was treated with [14]aneS_4. Its IR spectrum and properties such as reactivity or air-sensitivity indicate the presence of Se_2N_2 in solution. Upon prolonged stirring it dimerizes to Se_4N_4. Another proposed pathway towards selenium-containing polymeric chalcogen nitride is the thermolysis of 1,5-$Se_2S_2N_4$.[103]

4 Silver and copper complexes of selenium diimides

4.1 Background

Sulfur and selenium diimides can be prepared by treating primary amines with sulfur(IV) or selenium(IV) halides.[7-8] Sulfur diimides are thermally stable monomers and have extensive coordination chemistry. By contrast, selenium diimides are thermally unstable.[7-8,104-105] ^{t}BuNSeN^{t}Bu for example will undergo decomposition to ^{t}BuNN^{t}Bu and various cyclic selenium imides. AdNSeNAd is the only selenium diimide for which a crystal structure has been determined.[106] Several chelating complexes of selenium diimides have been prepared with $SnCl_4$,[107] $[PdCl_2(NCPh)_2]$,[108] and $CoCl_2$.[109] They have all been structurally characterized.

Unlike the lighter congeners, diimides of tellurium form dimers.[109] These dimers coordinate to metal centers through exocyclic nitrogen atoms in similar fashion as does the selenium diimides. Tellurium diimide dimer (^{t}Bu)NTe(μ-N^{t}Bu)$_2$TeN(^{t}Bu) forms a 1:1 complex $[CoCl_2\{N,N'\text{-}Te_2(N^{t}Bu)_4\}]$ with $CoCl_2$. The isostructural complex $[HgCl_2\{N,N'\text{-}Te_2(N^{t}Bu)_4\}]$ is obtained from the reaction of $\{Li_2[Te(N\text{-}^{t}Bu)_3]\}_2$ with $HgCl_2$.[110] The tellurium diimide also forms complexes with $Ag(CF_3SO_3)$ and $Cu(CF_3SO_3)$.[111-112] The complex $\{[Te(\mu\text{-}N^{t}Bu)]_2(\mu\text{-}N^{t}Bu)_2Ag\text{-}(O_3SCF_3)\}_2$ has two Ag^+ ions bridging two tellurium diimide dimers.[112] The complex has a short Ag···Ag distance of 2.888(2) Å that suggests d^{10}-d^{10} closed-shell interaction.

4.2 Theoretical analysis of the structures and d^{10}-d^{10} interactions[II]

In the reaction between two selenium diimides (RNSeNR, R = ^{t}Bu, Ad) and metal trifluorosulfonates (M = Ag, Cu), four new metal complexes with M-M d^{10}-d^{10} interactions have been synthesized.[II] The structures for the metal complexes containing adamantyl selenium diimide are shown in Figures 4a and 4b; and those containing *t*-butyl selenium diimide in Figures 4c and 4d.

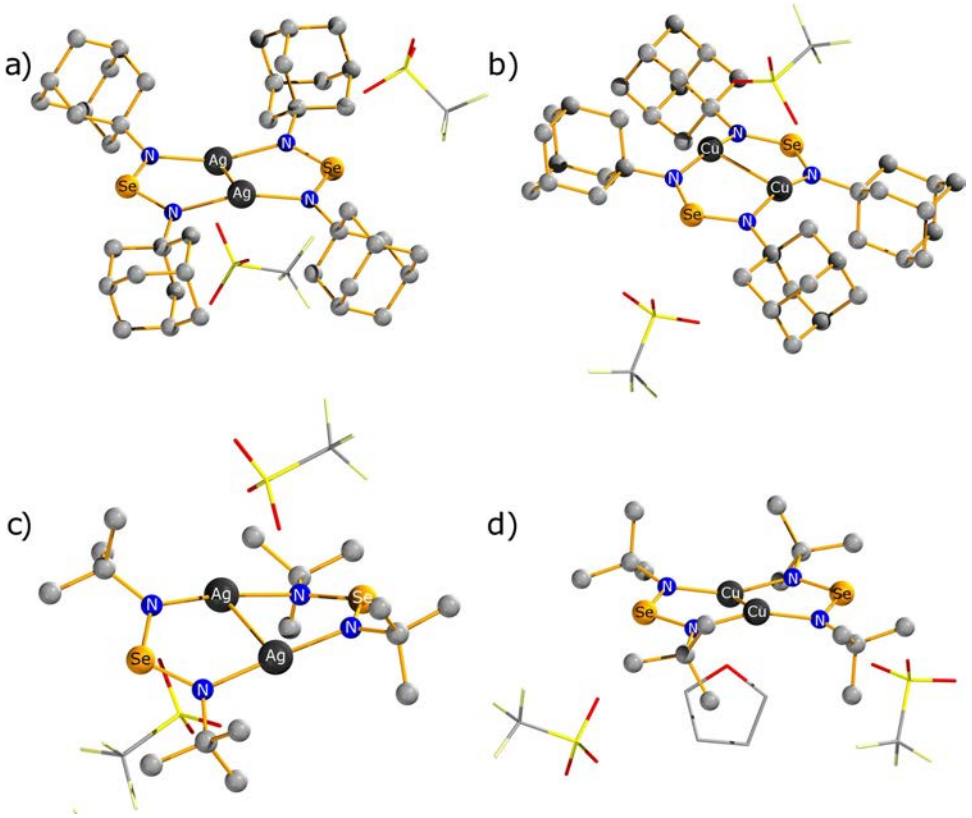

Figure 4. The molecular structures of $[M_2\{\mu\text{-N,N'-Se(NR)}_2\}_2](O_3SCF_3)_2$ (M = Ag, Cu; R = Ad, ^{t}Bu). Redrawn from crystallographic information.[II]

Structures in Figure 4 show that the bicyclic complex can adopt at least three different stereoisomeric structures.[II] Depending on the coordination of solvent molecules and counter anions in the crystal structure, the metallacyclic complex can adopt out-of-plane (Fig. 4a, 4d), bent (Fig. 4b) or twisted (Fig. 4c) geometries. In the out-of-plane isomer the metal atoms bend slightly out of the selenium diimide plane.

PBE/def-TZVP optimized geometries for the cations in gas phase (Fig. 5) show that the dications adopt either a planar or twisted geometry.[II] The potential energy surface for these metal complexes must be very shallow, and small changes in solvent interactions, packing or size of the organic groups affect the geometry more than electronic effects.

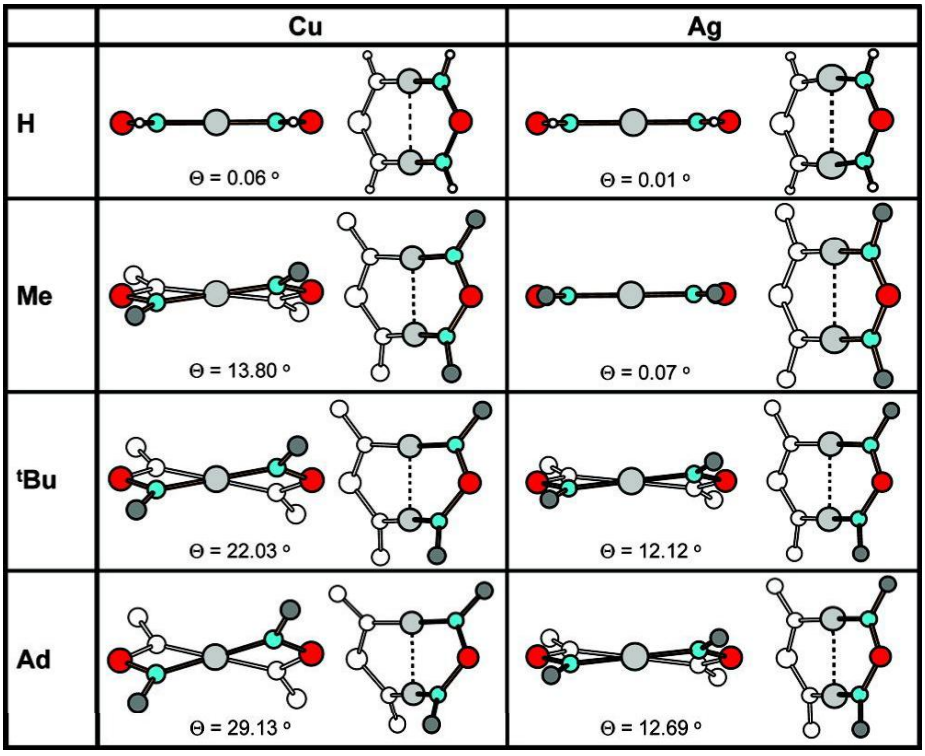

Figure 5. Twisting of the complex framework is respect to the organic group.[II] The angle Θ ($D_2M\cdots MD_2$) indicates the twisting of the complex from planarity. "Reprinted with permission from *Inorg. Chem*. **2009**, *48*, 6271-6279. Copyright 2009 American Chemical Society."

Atomic partial charges for the metallacycles have been calculated with PBE/def-TZVP based on the AIM method. These results are tabulated in Tables 2 and 3 alongside with bond critical point (BCP) electron density values and the delocalization indices for the M-M interaction.

Table 2. BCP electron density and delocalization indices (DI) in the Cu···Cu contact, and the partial charges (AIM) on the corresponding metal atom of $[Cu_2\{\mu\text{-}N,N'\text{-}Se(NR)_2\}_2]^{2+}$ cations.[II]

	exp. d (Cu···Cu)	theor. d(Cu···Cu)	ρ (e Å^{-3})	DI	Charge
R = H		2.713	0.027	0.300	0.718
R = Me		2.612	0.032	0.339	0.658
R = ^{t}Bu	2.556(2)-2.569(2)	2.576	0.034	0.339	0.624
R = Ad	2.531(1)	2.551	0.035	0.336	0.610

ρ is the electron density at the BCP, DI is the estimated bond order

Table 3. BCP electron density and delocalization indices (DI) in the Ag···Ag contact, and the partial charges (AIM) on the corresponding metal atom of $[Ag_2\{\mu\text{-}N,N'\text{-}Se(NR)_2\}_2]^{2+}$ cations.[II]

	exp. d (Ag···Ag)	theor. d(Ag···Ag)	ρ (e Å^{-3})	DI	Charge
R = H		2.924	0.026	0.259	0.661
R = Me		2.851	0.030	0.289	0.611
R = ^{t}Bu	2.7384(9)	2.816	0.032	0.293	0.565
R = Ad	2.751(2)	2.816	0.032	0.294	0.545

ρ is the electron density at the BCP, DI is the estimated bond order

In all cases, the AIM method finds an interaction which corresponds to bond order of roughly 0.3. A quite clear trend is the lowering of partial charge on the metal in connection to the electron donating ability of the organic group that increases in order of H > Me > ^{t}Bu > Ad. This charge-transfer effect is analogous to what was observed in case of the nitrosonium adducts of the disulfides (see Chapter 5 below). The lowering of the PBE/def-TZVP partial charges correlates with the shortening of the metal-metal contact and with the increase in the electron density at the M-M BCP.

Comparison of HF, PBE and MP2 optimized structures and bonding in the case of the $[Cu_2\{\mu\text{-}N,N'\text{-}Se(NH)_2\}_2]^{2+}$ model complex is shown in Table 4. Good qualitative agreement can be seen between DFT and MP2 theories. HF on the other hand does not show any real attraction between the metal atoms.

Table 4. AIM analysis of of $[Cu_2\{\mu\text{-}N,N'\text{-}Se(NH)_2\}_2]^{2+}$ for selected BCPs, calculated with def2-TZVP basis set.

		Bond (Å)	ρ (e Å^{-3})	DI	Charge
Cu1-Cu2	HF	3.190	0.008	0.051	0.708
	PBE	2.727	0.026	0.293	0.643
	MP2	2.793	0.023	0.200	0.631
N3-Cu1	HF	2.060	0.072	0.593	-1.920
	PBE	1.883	0.112	0.692	-1.150
	MP2	1.857	0.118	0.601	-1.220
H4-N3	HF	1.007	0.343	0.740	0.431
	PBE	1.032	0.317	0.754	0.378
	MP2	1.031	0.313	0.641	0.412

ρ is the electron density at the BCP, DI is the estimated bond order

These kinds of metal-metal interactions have extensively been studied and analyzed by Pyykkö *et al.*[113-114] The existence of the d^{10}-d^{10} interactions in the gold complexes is clear, but those in silver and copper complexes are somewhat controversial. The close intermetal distances can be conceived to be due to the strong anisotropy in the atomic electron density distribution. The attractive interactions arise from the closed-shell effects that can only be described by considering the electron correlation. Post-HF methods are best suited for the task. DFT can be problematic as dispersive second-order properties are not explicitly included in the theoretical formulation.[110] Most DFT methods may even get the sign of the interaction energy wrong near to the van der Waals energy minimum.[115]

Within the formalism of the AIM theory a BCP is found with all three methods (HF, PBE and MP2 in Table 4) for the $[Cu_2\{\mu\text{-}N,N'\text{-}Se(NH)_2\}_2]^{2+}$. In the case of the HF results this cannot be taken as an indication of attraction. It therefore also creates some ambiguity on the interpretation of the PBE results, which indicate attractive interaction at the PBE level of theory. Higher level computations, such as second-order approximate coupled cluster CC2/def2-TZVPP computations on the $[Cu_2\{\mu\text{-}N,N'\text{-}Se(NH)_2\}_2]^{2+}$ model predicted the Cu-Cu distance to be 2.60 Å.[II] Comparable computations with PBE/def2-TZVPP and MP2/def2-TZVPP result in Cu-Cu distances of 2.73 and 2.77 Å.

5 Reactions and adducts of nitrosonium

5.1 Background

The nitrosonium cation and nitric oxide are important as biological messengers in both plants and animals.[116] Nitric oxide reacts rapidly to form NO_x compounds which subsequently react with cellular amines or thiols, or hydrolyze to nitrites or nitrates. NO can directly coordinate with iron centers in proteins affecting its activity in the biological systems. NO easily undergoes redox reactions. Oxidation to the nitrosonium cation (NO^+) may be mediated by Fe(III) containing proteins. NO^+ participates in the electrophilic attack on the reactive centers where thiol groups are most reactive. These reversible reactions affect the activity of proteins and enzymes and can thus be a part of an important biological signaling mechanism. The biological role of the monooxidonitrate anion (NO^-) is unclear, but it is suspected to have a role in the oxidation reactions.

The biological importance of nitric oxide and its redox forms necessitates deeper understanding of the mechanisms of its reactions.[117] Towards this goal, the structure and stability trends of nitrosonium adducts with cytosine, uracil, thymine, and adenine bases have been investigated with MP2-level computations. *n*-Adducts were generally found to be more stable than π-adducts.

The pathway of the reaction of nitrosonium triflate and organic dichalcogenides depends on the chalcogen element. In case of diselenides and ditellurides (at -25 or -30 ˚C), a one-electron oxidation occurs with the generation of an $(ER)_2^+$ (E=Se, Te) cation.[118,III] In the solid state they

dimerize to form cyclic, planar $(ER)_4^{2+}$, which contain weak Se···Se and Te···Te contacts between the monomer components.[118] The nitrosonium triflate is unable to oxidize disulfides but forms adducts instead.[III] At higher temperatures, similar reactions with nitrosonium and a mixture of two organic disulfides result in disproportionation and the cleavage of the S-S bond.[119-120]

5.2 Synthesis and theoretical analysis[III]

The synthesis of the nitrosonium adducts of three organic disulfides (R=*neo*-pentyl, Me, Et) have been carried out, as shown in scheme 1.[III]

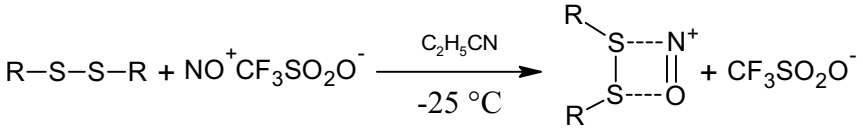

Scheme 1

The reaction affords a red solution from which green crystals can be grown at -80 °C, while the solution turns yellow. The observed color change is reversible with the resolvation of the crystals.[III] Reactions with dimethyl and diethyl disulfides also resulted in colored solutions, although no crystals could be isolated. $[C_{10}H_{22}S_2 \bullet NO^+TfO^-]$ crystallized in the C_2/c space group. The asymmetric unit is shown in Figure 6.

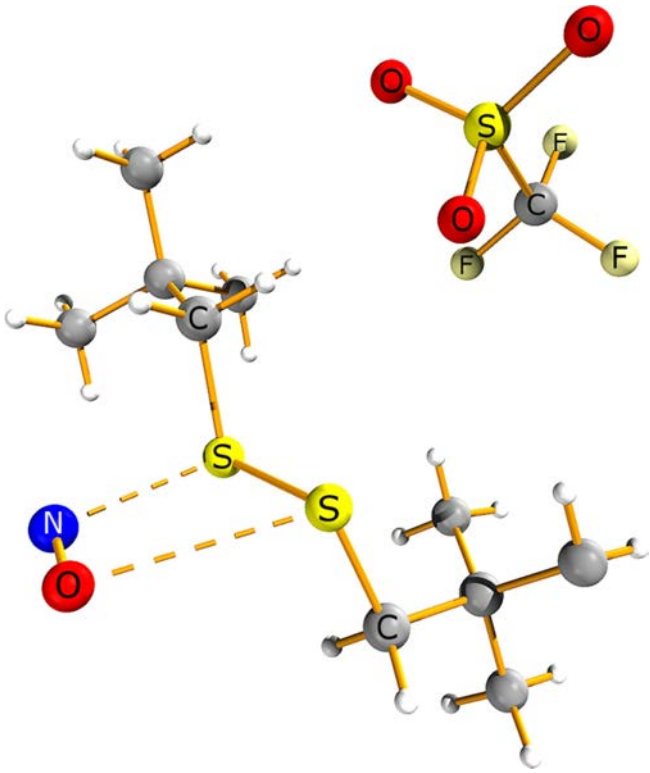

Figure 6. Molecular structure of the di-*neo*-pentyl nitrosonium adduct with a triflate counteranion. Redrawn from crystallographic information.[III]

The adduct formation leads to a notable change in the R-S-S-R torsion angle from that of *ca.* 90˚.[III] In the di-*neo*-pentyl disulfide nitrosonium adduct, the angle is 160.20(2)˚. The S-S bond length also becomes shorter and the nitrosonium N-O bond length is elongated.

DFT calculations (M06L/def2-TZVPP) were performed to understand better the bonding and stability of the nitrosonium adducts.[III] In addition to methyl, ethyl and *neo*-pentyl disulfides, for which there is experimental information; also dicyano, bis(trifluoromethyl), bis(*p*-pyridyl), hydrogen disulfides, diphenyl, bis(2-propyl) and adamantyl disulfides were

considered. The organic groups were chosen to encompass a wide range of electron-withdrawing and -donating groups. The computed Gibbs energies for the series of adduct-formation reactions are presented in Table 5. It can be seen that electron-donating organic groups stabilize the adduct, whereas electron-withdrawing groups have a reverse effect. In case of the phenyl substituent, the resonance effects enhance the stability of the adduct.

Table 5. Change in standard Gibbs energy (kJ/mol) for the reaction $R_2S_2 + NO^+ \Rightarrow [R_2S_2\text{-}NO]^+$.[III] (M06L/def2-TZVPP, CPCM-solvation, T = 298.15 K)

CN	CF_3	*p*-pyr	H	Ph	2-Prop	Me	Et	*neo*-Pent	Ad
+24	-3	-41	-58	-66	-74	-82	-87	-89	-98

dicyano (CN), trifluoromethyl (CF_3), phenyl (Ph), 2-propyl (2-prop), *neo*-pentyl (*neo*-Pent), adamantyl (Ad)

AIM atomic partial charges support this stability trend.[III] During the adduct formation, electron density is transferred from the S-S HOMO orbital to the nitrosonium LUMO orbital. Good electron-donating groups support this charge transfer and lower the partial charges in sulfur atoms. Strong electron-withdrawing groups, however, compete with nitrosonium in the charge transfer resulting in very high partial charges for sulfur atoms. The computed partial charges for the whole series are shown in Table 6. The adduct stability correlates well with the magnitude of the charge transfer to the nitrosonium cation from the disulfide.

Table 6. Partial charges (AIM) for three partitions of the adduct: two sulfur atoms (S_x), organic groups (R_x) and the nitrosonium.[III] For comparison, the partial charges for free trifluoromethyl and adamantyl disulfides are shown.

	S1	S2	R1	R2	N	O	N-O
CN	+0.658	+0.633	-0.446	-0.471	+0.942	-0.316	+0.626
CF_3	+0.191	+0.159	+0.054	+0.025	+0.895	-0.325	+0.570
p-Pyr	+0.213	+0.158	+0.112	+0.085	+0.778	-0.345	+0.433
H	+0.274	+0.219	+0.050	+0.029	+0.778	-0.351	+0.428
Ph	+0.208	+0.115	+0.180	+0.151	+0.708	-0.363	+0.345
2-Prop	+0.152	+0.081	+0.218	+0.189	+0.721	-0.362	+0.359
Me	+0.192	+0.117	+0.180	+0.157	+0.715	-0.362	+0.354
Et	+0.153	+0.076	+0.221	+0.197	+0.715	-0.361	+0.354
neo-Pent	+0.142	+0.075	+0.233	+0.201	+0.709	-0.360	+0.349
Ad	+0.087	+0.012	+0.300	+0.262	+0.704	-0.364	+0.340
CF_3 (free)	+0.114	+0.114	-0.115	-0.115	-	-	-
Ad (free)	-0.114	-0.114	+0.115	+0.115	-	-	-

dicyano (CN), trifluoromethyl (CF_3), phenyl (Ph), 2-propyl (2-prop), *neo*-pentyl (*neo*-Pent), adamantyl (Ad)

The computed and experimental structural parameters for the free organic disulfides and their respective adducts are summarized in Tables 7 and 8, respectively.[III] The trends described above are also apparent in the experimental metrical values. The S-S bond is shortened by the adduct formation. When the organic substituent is electron-donating (2-Prop, Me, Et, *neo*-Pent, Ad) the shortening is more pronounced and consequently the stability of the cation is enhanced. In case of the electron-withdrawing groups (CN, CF_3, *p*-pyridyl, Ph), the S-S bond becomes longer. The phenyl group shows noticeable resonance resulting in extended electron delocalization in the entire disulfide framework.[III] The delocalization renders the adduct significantly more stable than what is expected based on the weakening of the S-S bond.

Table 7. Calculated bond lengths (Å) and the R-S-S-R torsion angle (°) for selected free R_2S_2.[III]

R		CN	CF_3	*p*-Pyridyl [a]	H [b]	Ph [c]	2-Prop [d]	Me [a]	Et	*neo*-Pent	Ad
S1-S2	calc.	2.071	2.013	2.020	2.043	2.017	2.021	2.030	2.030	2.028	2.033
	exp.			2.032(1)	2.0610(3)	2.0230(8)	2.0303(8)	2.03(1)			
R1-S1	calc.	1.680	1.840	1.772	1.343	1.781	1.847	1.809	1.827	1.838	1.858
	exp.			1.780(2)	1.3421(5)	1.7894(6)	1.830(2)	1.803(3)			
R2-S2	calc.	1.680	1.840	1.772	1.343	1.781	1.847	1.809	1.827	1.838	1.858
	exp.			1.7870(2)	1.3421(5)	1.7876(3)	1.838(5)	1.805(3)			
R1-S1-S2-R2	calc.	89.0	95.5	84.4	90.3	86.0	91.2	84.2	84.9	82.0	109.0
	exp.			84.0(1)	90.76(6)	84.99	89.0(1)	86.1(1)			
ρ [e]	calc.	0.143	0.157	0.156	0.149	0.156	0.155	0.153	0.153	0.153	0.151

[a] For experimental bond parameters, see Ref. 121. [b] For experimental bond parameters, see Ref. 122. [c] For experimental bond parameters, see Ref. 123. [d] For experimental bond parameters, see Ref. 124. [e] ρ is the electron density at the bond critical point of the S-S bond.

Table 8. Calculated bond lengths (Å) and the R-S-S-R torsion angle (°) for selected $[R_2S_2\text{-}NO]^+$ cations.[III]

R		CN	CF_3	*p*-Pyridyl	H	Ph	2-Prop	Me	Et	*neo*-Pent	Ad
S1-S2	calc.	2.092	2.011	2.023	2.026	2.040	2.014	2.018	2.014	2.014	2.004
	exp.									2.0105(6)	
R1-S1	calc.	1.674	1.883	1.771	1.344	1.760	1.844	1797	1.822	1.827	1.869
	exp.									1.8121(6)	
R2-S2	calc.	1.673	1.870	1.773	1.342	1.775	1.842	1.802	1.825	1.827	1.870
	exp.									1.8226(5)	
S1-N	calc.	2.665	2.569	2.509	2.493	2.453	2.438	2.454	2.44	2.425	2.438
	exp.									2.3035(7)	
S2-O	calc.	3.020	2.978	2.950	2.857	2.934	2.916	2.876	2.882	2.907	2.903
	exp.									2.8592(7)	
N-O [a]	calc.	1.087	1.092	1.103	1.104	1.111	1.110	1.110	1.110	1.111	1.111
	exp.									1.1215(3)	
R1-S1-S2-R2	calc.	145.0	125.3	143.4	166.9	164.2	157.0	161.0	153.3	149.2	141.2
	exp.									160.20(2)	
ρ [b]	calc.	0.139	0.159	0.156	0.155	0.152	0.159	0.159	0.159	0.159	0.160

[a] The computed N-O bond length of free NO^+ is 1.059 Å. [b] ρ is the electron density at the bond critical point of the S-S bond.

The predicted shortening of the S-S bond is largest in the case of the diadamantyl disulfide adduct.[III] Upon adduct formation, the S-S bond shortens from 2.033 Å to 2.004 Å and the partial charge of nitrosonium ion decreases from +1.00 to +0.34.

The shortening of the S-S bond can qualitatively be explained in terms of orbital interactions.[III] The HOMO and HOMO-1 of the disulfide have mainly the sulfur p-orbital character. These orbitals have different nodal structures. The HOMO is antibonding, whereas the HOMO-1 is bonding with respect to the S-S bond. The R-S-S-R torsional angle of *ca.* 90˚ minimizes the overlap of the sulfur p-orbitals rendering the HOMO and HOMO-1 essentially non-bonding in free disulfide. The respective bonding or anti-bonding character of HOMO-1 or HOMO is most pronounced if the disulfide would adopt fully planar conformation in respect the R-S-S-R torsional angle. As an example, MeSSMe can be forced to adopt a fully planar conformation (the R-S-S-R torsional angle is either 0 ^{o} or 180 ^{o}) as shown in Figure 7. There is no net gain in energy as when the HOMO-1 becomes fully bonding; it is countered by the fully antibonding HOMO. Instead, the energy of the system increases as the electron density is restricted in a more crowded space. In $MeSSMe^{+}$ cation the HOMO orbital is split in SOMO and LUMO with the loss of an electron. In this case the SOMOs that correspond to the MeSSMe HOMO-1 have higher occupancy than the lone SOMO and the planar geometry becomes energetically favorable (see Fig. 8).

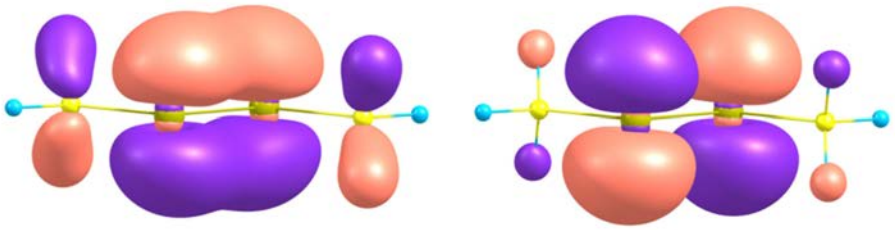

Figure 7. The HOMO-1 (left) and HOMO (right) of MeSSMe molecule planar conformation. Loss of electron density from the HOMO renders the planar geometry energetically more favorable.[III] "Reprinted with permission from *Eur. J. Inorg. Chem.* **2011**, 4970-4977. Copyright 2011 John Wiley and Sons."

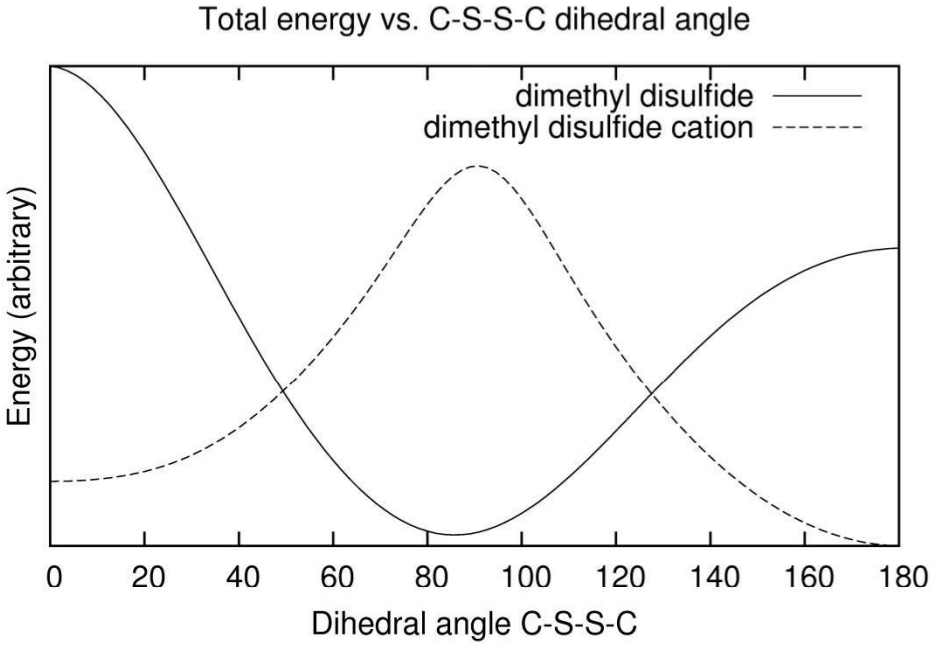

Figure 8. The energy profile of MeSSMe and $MeSSMe^{+}$ in respect to C-S-S-C dihedral angle (M06L/def2-TZVPP). The energy scales are arbitrary. If the electron density donation from the disulfide HOMO to the nitrosonium cation is sufficiently large, the disulfide would adopt fully planar geometry (See Fig. 7).[III]

The third important orbital is the LUMO of the nitrosonium cation.[III] This is fully antibonding with respect to the N-O bond. During the adduct formation, electron density is transferred from the disulfide HOMO to the nitrosonium LUMO. The addition of electron density to the nitrosonium LUMO also weakens the N-O bond. The N-O bond lengths of the different adducts together with that predicted for the free NO^+ is shown in Table 8.

6 Hybrid chalcogenidoborate anions

6.1 Background

The chalcogenidoborate anions considered in this chapter are planar boron anions with formal sp^2 hybridization on the boron atom.[IV] These can be considered to be building blocks for larger clusters such of B_2S_3[125] or B_8S_{16}[126] as illustrated in Figure 9a. The four building blocks for the structures of the anions are shown in Figure 9b.

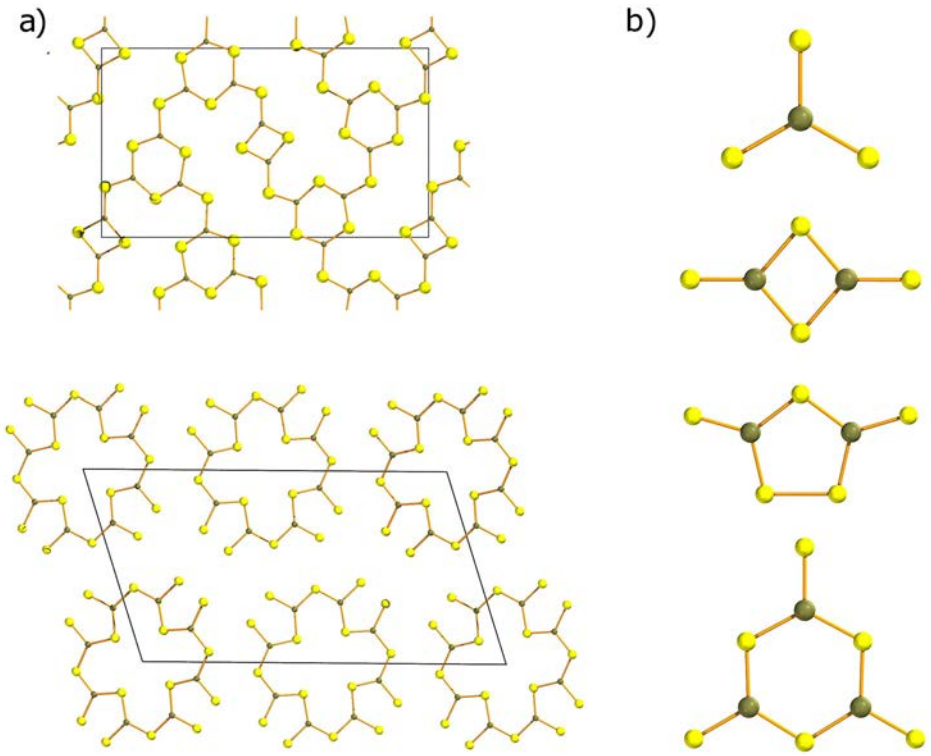

Figure 9. a) Crystal structures of B_2S_3 and B_8S_{16} b) Sulfidoborate anions.[IV] The crystal structures are redrawn from crystallographic information in Refs. (125) and (126).

Large number of crystal structures are known for compounds containing the BS_3^{3-} [126-144] frame-work, whereas only a few are known for BSe_3^{3-} [131,134,144-147], $B_2S_4^{2-}$ [148], $B_2S_5^{2-}$ [149] and $B_3S_6^{3-}$.[128,150-152] The BSe_3^{3-} is the only known homoleptic selenidoborate anion structure characterized while no hybrid chalcogenidoborate anions have been reported. A number of new crystal structures containing BS_3^{3-} anion has recently been reported.[135-143] The B-S bond lengths in different BS_3^{3-} structures show a range of 1.770(4)-1.913(11) Å.

Surprisingly long B-S bond lengths in BS_3^{3-} are reported for $Dy_9B_5S_{21}$ (1.913(11) Å) and $Ho_9B_5S_{21}$ (1.909(3) Å) by Kniep *et al.*[143] The $RE_9[BS_3]_2[BS_4]_3S_3$, (RE=Dy-Lu), are isomorphic with $Ce_6Al_{3.33}S_{14}$. In this structure type, systematic presence of vacancies in the crystal lattice is necessary in order to balance the charges. Quantum mechanical analysis revealed that in these RE structures every third boron atom site in $[BS_3]^{3-}$ is replaced by a boron vacancy (the $[\square S_3]^{6-}$ unit). Boron atoms in two other BS_3^{3-} units are displaced from the plane defined by the sulfur atoms by 0.217-0.065 Å. The S-S contacts in these trigonal units are also predicted to be slightly elongated to lower the repulsion from the large partial charges in the units containing the boron vacancy. It may be that the abnormally long B-S bonds result from minimization of the Coulomb repulsion to counterbalance the large negative charges in the partially vacant BS_3^{3-} units. The B-S bond lengths in the BS_3^{3-} anions of $RE_9[BS_3]_2[BS_4]_3S_3$ show a range 1.762(7)-1.913(11)[143] Å, whereas the structures of related salts exhibit a variation range of 1.770(4)-1.861(8)[153-154] Å.

6.2 Theoretical analysis of the chalcogenidoborate anions[IV]

Hybrid chalcogenidoborates of sulfur and selenium still remain elusive. The theoretical predictions presented in paper IV are still the only information available on these compounds.[IV] The stability and structural trends of all chalcogenidoborate anions of series $BSe_xS_{3-x}^{3-}$ (x = 0-3), $B_2Se_xS_{4-x}^{2-}$ (x = 0-4), $B_2Se_xS_{5-x}^{2-}$ (x = 0-5), and $B_3Se_xS_{6-x}^{3-}$ (x = 0-6) have been considered. All the computed anions were found to adopt fully planar geometry. For each of the four structural frameworks, the increase in the selenium content in the anions lowers the total binding energies. The location of the selenium atom in the framework was found to influence the stability of the anion. Generally those hybrid chalcogenidoborates, where the selenium is exocyclic, are more stable than those, where selenium is a part of the ring.

The $B_3Se_xS_{6-x}^{3-}$ anions are considered here as an illustrative example (see Figure 10).[IV] The relative stabilities of the isomers of the $B_3Se_xS_{6-x}^{3-}$ anions are shown in Figure 11.

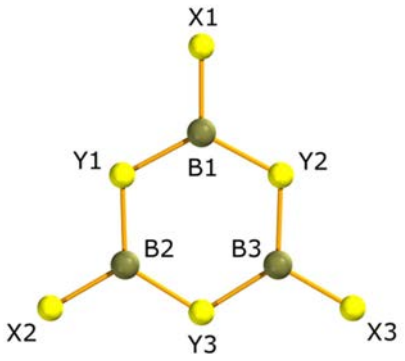

Figure 10. Labeling of atoms in $B_3S_6^{3-}$.[IV]

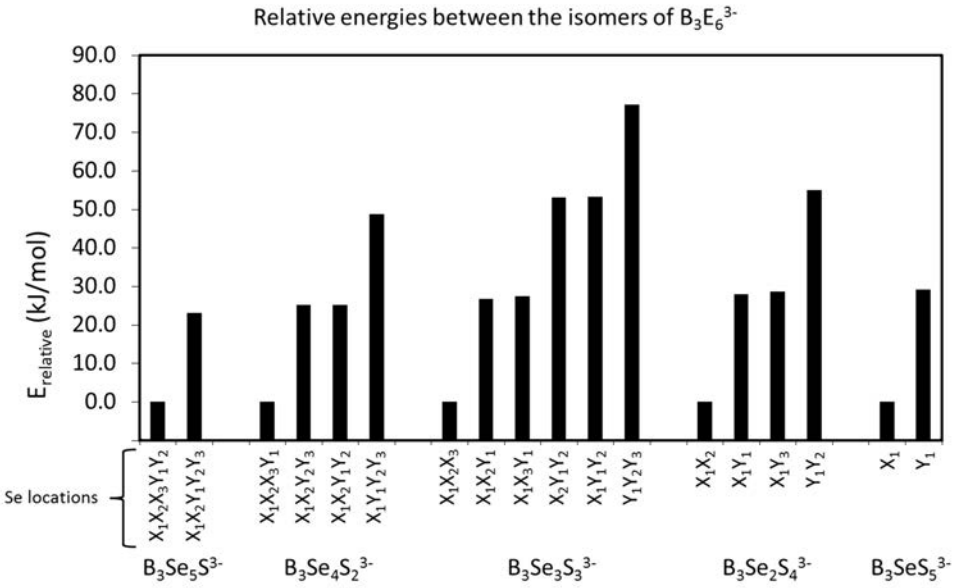

Figure 11. Stability trends of $B_3Se_xS_{6-x}^{3-}$ (x = 0-6) depending on the location of selenium atom (MP2/6-311+G(2d)). See Figure 10 for the definition of the labeling.[IV]

For example, in X_1-$B_3SeS_5^{3-}$ isomer; with the only selenium in exo-position, is predicted to be more stable than the Y_1 isomer with one selenium in the ring framework. Same trend can be observed for all the 5 sets of hybrid chalcogenoborate anions of series $B_3Se_xS_{6-x}^{3-}$. Compared to $B_3S_6^{3-}$ and $B_3Se_6^{3-}$, the B-S bonds in hybrid $B_3Se_xS_{6-x}^{3-}$ are slightly shortened, whereas the B-Se bonds are elongated.[IV] This is consistent with the corresponding increase of electron density at B-S bond critical points (BCP) and its decrease at B-Se BCPs based on AIM analysis. Because sulfur is slightly more electronegative than selenium, it draws more electron density from boron than selenium. These effects on structure and bonding are illustrated in Figure 12 for the $BSe_xS_{3-x}^{3-}$. In the homoleptic BS_3^{3-} the electron density value in the B-S bond is 0.135, whereas it

increases to 0.144 in $BSeS_2^{3-}$, to 0.150 in BSe_2S^{3-} and finally up to 0.150 in BSe_2S^{3-}. Likewise the electron density value in the B-Se bonds drop from 0.121 down to 0.104 when going from BSe_3^{3-} to $BSeS_2^{3-}$. The electron density trends also correlate with changes in bond lengths. B-S bond length shortens from 1.87 Å in BS_3^{3-} down to 1.81 Å in BSe_2S^{3-}.

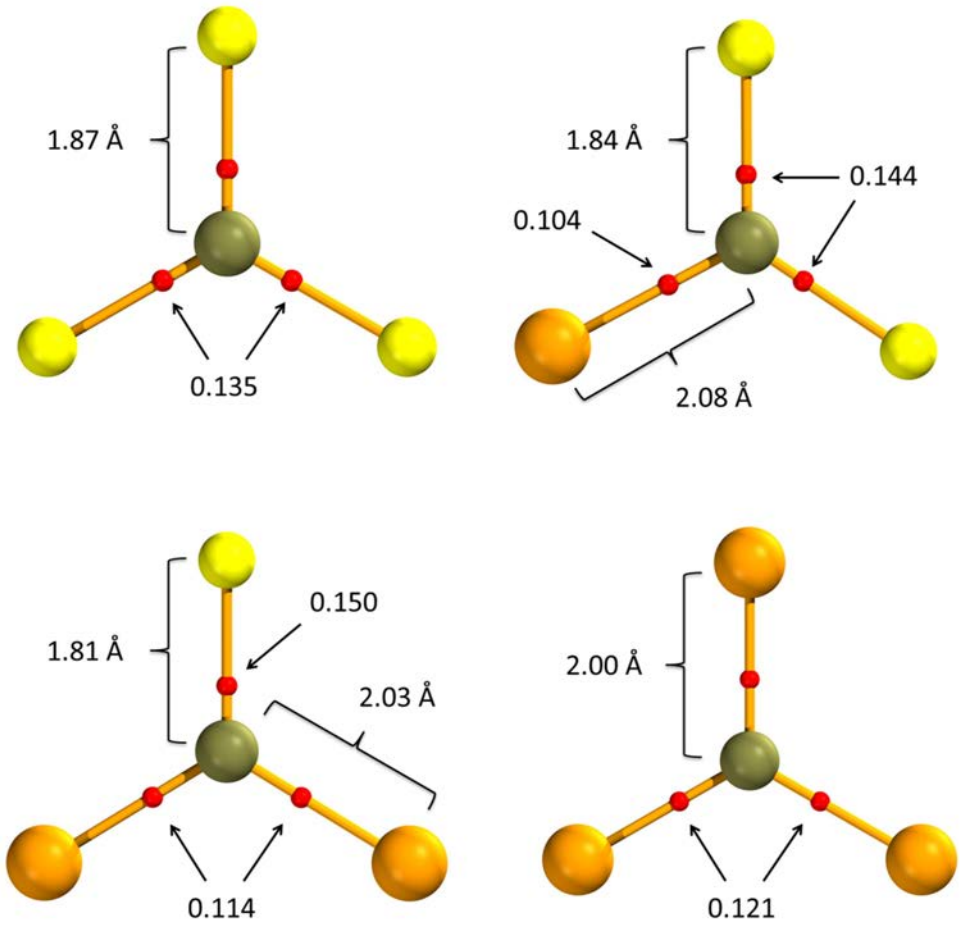

Figure 12. Electron density values at bond critical points (red) and B-E bond lengths in $BSe_xS_{3-x}^{3-}$ (x = 0-3, S yellow, Se orange) (MP2/6-311+G(2d)).[IV]

In the theoretical study of chalcogenoborate anions of sulfur and selenium, novel homoleptic selenidoborate anions and hybrid chalcogenidoborate anions have been investigated.[IV] Experimentally only the sulfidoborate anions and the smallest investigated selenidoborate anion BSe_3^{3-} are known. All the investigated anions would seem plausible. The hybrid chalcogenoborate anions with selenium in exo-positions are predicted to have higher stability than those anions with selenium within the ring framework.

7 Conclusions and outlook

Theoretical analysis of the bonding, structural properties, and reaction mechanisms has been performed for several chalcogen-containing molecules. MD simulations are an efficient method in the study of solid-state topochemical reactions. AIM has successfully been used to investigate the bonding trends comprising chalcogenidoborates, NO^+ adducts of organic disulfides, and d^{10}-d^{10} closed-shell interactions in metallacyclic selenium diimide complexes.

The molecular dynamics simulations on the topochemical polymerization reaction of S_2N_2 proved to be a powerful tool for the study of reactions of crystalline materials. The inclusion of proper chemical environment in the form of a periodic simulation cell and the inclusion of the thermal motion allowed for a more realistic investigation of the reaction pathways than has been possible in the earlier theoretical works on the reaction mechanism, which have involved isolated gaseous molecules. The polymerization was found to be initiated by a cleavage of a single S-N bond of one S_2N_2 ring molecule. The reaction then quickly propagates along the crystallographic *a* axis. The side-reactions in the simulations explain the observed polymorphism. With a working model for the simulation of S_2N_2 rings, a clear future target is to continue the work with the heavier chalcogens. Se_2N_2 and $SSeN_2$ rings are the prime targets for future studies. Tellurium-containing chalcogen nitride rings are also potential targets for investigation.

The metal-metal interactions and structural properties of dinuclear copper(I) and silver(I) selenium diimides were investigated. These metallacyclic complexes exhibit d^{10}-d^{10} closed-shell interactions. Theoretical analysis based on AIM theory on the metal-metal interaction suggests an attractive interaction in both copper and silver complexes. The theoretical results indicate that the twisting of the bicyclic complex is related to the strength of the M-M interaction. This interaction strength is connected to the electron-donating abilities of the organic substituent of the selenium diimide. The twist may arise from minimization of the overlap of non-bonding orbitals concentrated in the metals. These interactions have been investigated extensively; but the definitive answer, especially in case of Cu···Cu d10 interactions, remains elusive. Continued research is needed to quantitatively identify the nature of the metal-metal interactions in the coinage metals and to be able to reliably identify when the attraction is a real closed-shell interaction and when it is caused by other effects.

Organic disulfides form adducts with nitrosonium cations. Qualitative analysis of molecular orbitals and electron density has been used to effectively explain the stability and structural trends of several adducts and have been compared with the structural information, where available. The adduct formation takes place through charge-transfer from the disulfide to the nitrosonium cation. The charge-transfer occurs between the disulfide HOMO and HOMO-1, mainly comprised of sulfur lone pair electrons, and the nitrosonium LUMO orbital. Electron-donating organic groups stabilize the adduct formation by compensating the loss of electron density of the sulfur atoms.

The structural trends and bonding properties of $BSe_xS_{3-x}^{3-}$ (x = 0-3), $B_2Se_xS_{4-x}^{2-}$ (x = 0-4), $B_2Se_xS_{5-x}^{2-}$ (x = 0-5), and $B_3Se_xS_{6-x}^{3-}$ (x = 0-6) anions have also been explored. These trigonal planar anions can be considered to be building blocks of larger chalcogenidoborate layers, for example, of B_2S_3 or B_8S_{16}. Large numbers of crystal structures are known, which exhibit the isolated BS_3^{3-} anion. Only a few salts containing a BSe_3^{3-} anion and only a handful for the larger $B_2S_4^{2-}$, $B_2S_5^{2-}$ and $B_3S_6^{3-}$ anions are known. Furthermore, no experimental or theoretical information exist for the mixed chalcogenidoborate anions. Homoleptic sulfidoborate anions were found to be more stable than the selenium analogs in all four structural motifs. In case of the hybrid species, increased selenium content destabilizes the anions. Exocyclic selenium was predicted to be more favorable than the atom, which is a part in the ring structure. The current computations indicate that in principle the synthesis of hybrid chalcogenidoborates should be plausible.

8 References

1. Chivers, T.; Konu, J. *Comments Inorg. Chem.* **2009***, 30*, 131-176 and references therein.
2. Pauling, L. *The Nature of the Chemical Bond*, 3rd ed.; Cornell University Press: Ithaca, New York, 1960.
3. Wheland, G. W. *J. Chem. Phys.* **1934**, *2*, 474-81 and references therein.
4. Gillespie, R. J. *J. Chem. Educ.* **1963***, 40*, 295-301.
5. Power, P. P. *Nature*, **2010***, 463*, 171-177.
6. Sekiguchi, A.; Kinjo, R.; Ichinohe, M. *Science* **2004***, 305*, 1755-1757.
7. Chivers, T. *A Guide to Chalcogen-Nitrogen Chemistry*; World Scientific Publishing Co, Inc.: Singapore, 2005.
8. Chivers, T.; Laitinen, R. S. In *Handbook of Chalcogen Chemistry*, Devillanova, F., Ed.; RSC Publishing: London, 2007; pp 223−285.
9. Banister, A. J.; Gorrell, I. B. *Adv. Mater.* **1998**, *10*, 1415−1429.
10. Kelly, P. F.; King, R. P. S.; Mortimer, R. J. *Chem. Commun.* **2008**, 6111−6113.
11. Kwon, Y. H.; Kim, J. Y.; Kim, K. T.; Shin, H. C.; Cho, H. M.; Jung H. R. Eur. Pat. Appl. 2445043, 2012.
12. Koo, C. M.; Hong, S. M.; Baek, K. Y.; Hwang, S. S.; Park, Y. D.; Min, K. H.; Lee, J. H.; Lee, Y. J.; Jung, J. Y.; Lee, J. W. U.S. Pat. Appl. Publ. 20120286627, 2012.
13. Ma, Z. U.S. Pat. Appl. Publ. 20130020539 2013.
14. Ko, M. J.; Kim, H. G.; Lee, D. K.; Kim, K. K.; Kim, B. S.; Yoo, K. C. U.S. Pat. Appl. Publ. 20130056068 2013.

15. Kim, T. W.; Jeon, Y. P.; Choo, D. C. PCT Int. Appl. 2013019030 2013.
16. Shimuta, M.; Yasuda, S.; Mizuguchi, T.; Ohba, K.; Aratani, K. Eur. Pat. Appl. 2541555 2013.
17. Bleay, S. M.; Kelly, P. F.; King, R. S. P. *J. Mater. Chem.* **2010**, *20*, 10100−10102.
18. *SciFinder*; Chemical Abstracts Service: Columbus, OH, 2013; https://scifinder.cas.org (accessed April 18, 2013).
19. Razykov, T. M.; Ferekides, C. S.; Morel, D.; Stefanakos, E.; Ullal, H. S.; Upadhyaya, H. M. *Sol. Energy* **2011***, 85*, 1580-1608 and references therein.
20. *CP2K version 2.1.369 (Development Version)*; CP2K Developers Group, 2010. CP2K is freely available from http://www.cp2k.org/
21. VandeVondele, J.; Krack, M.; Mohamed, F.; Parrinello, M.; Chassaing, T.; Hutter, *J. Comput. Phys. Commun.* **2005**, *167*, 103−128.
22. Perdew, J. P.; Burke, K.; Ernzerhof, M. *Phys. Rev. Lett.* **1996**, *77*, 3865−3868.
23. Zhang, Y.; Yang, W. *Phys. Rev. Lett.* **1998**, *80*, 890.
24. Grimme, S. *J. Comput. Chem.* **2006**, 27, 1787−1799.
25. Grimme, S.; Antony, J.; Ehrlich, S.; Krieg, H. *J. Chem. Phys.* **2010**, *132*, 154104−19.
26. VandeVondele, J.; Hutter, J. *J. Chem. Phys.* **2007**, *127*, 114105−9.
27. Goedecker, S.; Teter, M.; Hutter, J. *Phys. Rev. B* **1996**, *54*, 1703−1710.
28. Hartwigsen, C.; Goedecker, S.; Hutter, *J. Phys. Rev. B* **1998**, *58*, 3641−3662.

29. Bussi, G.; Donadio, D.; Parrinello, M. *J. Chem. Phys.* **2007**, *126*, 014101-7.
30. Cohen, M. J.; Garito, A. F.; Heeger, A. J.; MacDiarmid, A. G.; Mikulski, C. M.; Saran, M. S.; Kleppinger, J. *J. Am. Chem. Soc.* **1976**, *98*, 3844−3848.
31. VandeVondele, J.; Hutter, J. *J. Chem. Phys.* **2003***, 118*, 4365-4369 and references therein.
32. Weber, V.; VandeVondele, J.; Hutter, J.; Niklasson, A. M. N. *J. Chem. Phys.* **2008***, 128*, 084113-9.
33. TURBOMOLE V5.10 2008, a development of University of Karlsruhe and Forschungszentrum Karlsruhe GmbH, 1989-2007, TURBOMOLE GmbH, since 2007; available from www.turbomole.com.
34. Gaussian 03, Revision D.02, Frisch, M. J.; Trucks, G. W.; Schlegel, H. B.; Scuseria, G. E.; Robb, M. A.; Cheeseman, J. R.; Montgomery, Jr., J. A.; Vreven, T.; Kudin, K. N.; Burant, J. C.; Millam, J. M.; Iyengar, S. S.; Tomasi, J.; Barone, V.; Mennucci, B.; Cossi, M.; Scalmani, G.; Rega, N.; Petersson, G. A.; Nakatsuji, H.; Hada, M.; Ehara, M.; Toyota, K.; Fukuda, R.; Hasegawa, J.; Ishida, M.; Nakajima, T.; Honda, Y.; Kitao, O.; Nakai, H.; Klene, M.; Li, X.; Knox, J. E.; Hratchian, H. P.; Cross, J. B.; Bakken, V.; Adamo, C.; Jaramillo, J.; Gomperts, R.; Stratmann, R. E.; Yazyev, O.; Austin, A. J.; Cammi, R.; Pomelli, C.; Ochterski, J. W.; Ayala, P. Y.; Morokuma, K.; Voth, G. A.; Salvador, P.; Dannenberg, J. J.; Zakrzewski, V. G.; Dapprich, S.; Daniels, A. D.; Strain, M. C.; Farkas, O.; Malick, D. K.; Rabuck, A. D.; Raghavachari, K.; Foresman, J. B.; Ortiz, J. V.; Cui, Q.; Baboul, A. G.; Clifford, S.;

Cioslowski, J.; Stefanov, B. B.; Liu, G.; Liashenko, A.; Piskorz, P.; Komaromi, I.; Martin, R. L.; Fox, D. J.; Keith, T.; Al-Laham, M. A.; Peng, C. Y.; Nanayakkara, A.; Challacombe, M.; Gill, P. M. W.; Johnson, B.; Chen, W.; Wong, M. W.; Gonzalez, C.; and Pople, J. A.; Gaussian, Inc., Wallingford CT, 2004.

35. Gaussian 09, Revision B.01, Frisch, M. J.; Trucks, G. W.; Schlegel, H. B.; Scuseria, G. E.; Robb, M. A.; Cheeseman, J. R.; Scalmani, G.; Barone, V.; Mennucci, B.; Petersson, G. A.; Nakatsuji, H.; Caricato, M.; Li, X.; Hratchian, H. P.; Izmaylov, A. F.; Bloino, J.; Zheng, G.; Sonnenberg, J. L.; Hada, M.; Ehara, M.; Toyota, K.; Fukuda, R.; Hasegawa, J.; Ishida, M.; Nakajima, T.; Honda, Y.; Kitao, O.; Nakai, H.; Vreven, T.; Montgomery, Jr., J. A.; Peralta, J. E.; Ogliaro, F.; Bearpark, M.; Heyd, J. J.; Brothers, E.; Kudin, K. N.; Staroverov, V. N.; Kobayashi, R.; Normand, J.; Raghavachari, K.; Rendell, A.; Burant, J. C.; Iyengar, S. S.; Tomasi, J.; Cossi, M.; Rega, N.; Millam, J. M.; Klene, M.; Knox, J. E.; Cross, J. B.; Bakken, V.; Adamo, C.; Jaramillo, J.; Gomperts, R.; Stratmann, R. E.; Yazyev, O.; Austin, A. J.; Cammi, R.; Pomelli, C.; Ochterski, J. W.; Martin, R. L.; Morokuma, K.; Zakrzewski, V. G.; Voth, G. A.; Salvador, P.; Dannenberg, J. J.; Dapprich, S.; Daniels, A. D.; Farkas, Ö.; Foresman, J. B.; Ortiz, J. V.; Cioslowski, J.; Fox, D. J. Gaussian, Inc., Wallingford CT, 2009.
36. M. Cossi, N. Rega, G. Scalmani, V. Barone, *J. Comput. Chem.* **2003**, *24*, 669.
37. Bader, R. F. W. *Atoms in Molecules: A Quantum Theory*; Oxford University Press; New York, 1990.

38. Popelier, P. *Atoms in Molecules: An Introduction*; Pearson Education Limited: England, 2000.
39. Bader, R. W. F; et. al. AIMPAC: A Suite of programs for the AIM theory; McMaster University: Hamilton, Ontario, Canada L8S 4M1, http://www.chemistry.mcmaster.ca/aimpac/
40. Biegler-König, F.; Schönbohm, J. *J. Comput. Chem.* **2002***, 23*, 1489-1494.
41. AIMAll (Version 11.03.14), Keith, T. A. TK Gristmill Software, Overland Park KS, USA, 2011 (aim.tkgristmill.com).
42. Matta, C. F.; Hernandez-Trujillo, J. *J. Phys. Chem. A* **2003***, 107*, 7496-7504.
43. Perdew, J. P.; Burke, K.; Ernzerhof, M. *Phys. Rev. Lett.* **1997***, 78*, 1396.
44. Weigend, F.; Häser, M. *Theor. Chem. Acc.* **1997**, *97*, 331-340.
45. Weigend, F.; Häser, M.; Patzelt, H.; Ahlrichs, R. *Chem. Phys. Lett.* **1998**, *294*, 143-152
46. Christiansen, O.; Koch, H.; Joergensen, P. *Chem. Phys. Lett.* **1995**, *243*, 409-418.
47. Hättig, C.; Weigend, F. *J. Chem. Phys.* **2000**, *113*, 5154-5161.
48. Hättig, C. J. Chem. Phys. **2003**, *118*, 7751-7761.
49. Hättig, C.; Hellweg, A.; Köhn, A. Phys. Chem. Chem. Phys. 2006, 8, 1159-1169
50. Schäfer, A.; Huber, C.; Ahlrichs, R. *J. Chem. Phys.* **1994**, *100*, 5829-5835.
51. Eichkorn, K.; Treutler, O.; Öhm, H.; Häser M.; Ahlrichs, R. *Chem. Phys. Letters* **1995**, *242*, 652660.

52. Eichkorn, K.; Weigend, F.; Treutler, O.; Ahlrichs, R. *Theor. Chem. Acc.* **1995**, *97*, 119-124.
53. Weigend, F. *Phys. Chem. Chem. Phys.* **2006***, 8*, 1057-1065.
54. Weigend, F.; Häser, M.; Patzelt, H.; Ahlrichs, R. *Chem. Phys. Letters* **1998***, 294*, 143-152.
55. Hättig, C. *Phys. Chem. Chem. Phys.* **2005**, *7*, 59-66.
56. Weigend, F.; Köhn, A.; Hättig, C. *J. Chem. Phys.* **2002**, *116*, 3175-3183.
57. Weigend, F.; Furche, F.; Ahlrichs, R. *J. Chem. Phys.* **2003**, *119*, 12753-12762.
58. Zhao, Y.; Truhlar, D. G. *J. Chem. Phys.* **2006**, *125*, 194101-18.
59. Feller, D. *J. Comp. Chem.* **1996***, 17*, 1571-1586.
60. Schuchardt, K. L.; Didier, B. T.; Elsethagem T.; Sun, L.; Gurumoorthi, V.; Chase, J.; Li, J.; Windus, T. L. *J. Chem. Inf. Model.* **2007***, 47*, 1045-1052.
61. Adamo, C.; Barone, V. *J. Chem. Phys.* **1999***, 110*, 6158-69.
62. Møller, C.; Plesset, M. S. *Phys. Rev.* **1934,** *46*, 618-622.
63. Krishnan, R.; Binkley, J. S.; Seeger, R.; Pople, J. A. *J. Chem. Phys.* **1980***, 72,* 650-654.
64. McLean, A. D.; Chandler, G. S. *J. Chem. Phys.* **1980***, 72*, 5639-5648.
65. Curtiss, L. A.; McGrath, M. P.; Blandeau, J. P.; Davis, N. E.; Binning, R. C.; Radom, Jr. L. *J. Chem. Phys.* **1995***, 103*, 6104-6113.
66. Burt, F. P. *J. Chem. Soc., Trans.* **1910**, *97*, 1171-4.
67. Greene, R. L.; Street, G. B.; Suter, L. *J. Phys. Rev. Lett.* **1975**, *34*, 577−579.
68. Love, P.; Kao, H. I.; Myer, G. H.; Labes, M.M *J. Chem. Soc., Chem. Commun.* **1978**, 301-302.

69. Chiag, C. K.; Druy, M. A.; Gau, S. C.; Heeger, A. J.; Loius, E. J.; MacDiarmid, A. G.; Park, Y. W.; Shirakawa, H. *J. Am. Chem. Soc.* **1978**, *100*, 1013-1015.
70. Haynes, W. M., Ed. *CRC Handbook of Chemistry and Physics*, 94th ed. [Online]; CRC Press: Boca Raton, FL, 2014; p 12-41.
71. Labes, M. M.; Love, P.; Nichols, L. F. *Chem. Rev.* **1979**, 79, 1−15.
72. Banister, A. J.; Hauptman, Z. V.; Rawson, J. M.; Wait, S. T. *J. Mater. Chem.* **1996**, *6*, 1161-1164.
73. Banister, A. J.; Hauptman, Z. V.; Passmore, J.; Wong, C-M.; White, P. S. *J. Chem Soc., Dalton Trans.* **1986,** 2371-2379.
74. Roesky, H. W.; Anhaus, J. *Chem. Ber.* **1982,** *115,* 3682-3684.
75. Baughman, R. H.; Apgar, P. A.; Chance, R. R.; MacDiarmid, A. G.; Garito, A. F. *J. Chem. Phys.* **1977**, *66*, 401−409.
76. Müller, H.; Svensson, S. O.; Birch, J.; Kvick, Å. *Inorg. Chem.* **1997**, *36*, 1488−1494.
77. Boudeulle, M. *Cryst. Struct. Comm.* **1975***, 4*, 9-12.
78. Heger, G.; Klein, S.; Pintschovius, L.; Kahlert, H. *J. Solid State Chem.* **1978***, 23*, 341-347.
79. Tuononen, H. M.; Suontamo, R.; Valkonen, J.; Laitinen, R. S. *J. Phys. Chem. A.* **2004,** *108***,** 5670-5677 and references therein.
80. Tuononen, H. M.; Suontamo, R.; Valkonen, J.; Laitinen, R. S.; Chivers, T. *J. Phys. Chem. A.* **2005**, *109*, 6309-6317.
81. Jung, Y.; Heine, T.; Schleyer, P. v. R.; Head-Gordon, M. *J. Am. Chem. Soc.* **2004**, *126*, 3132-3138.
82. Braida, B.; Lo, A.; Hiberty, P. C. *ChemPhysChem*, **2012**, *13*, 811-819.
83. Baughman, R. H.; Chance, R. R.; Cohen, M. J. *J. Chem. Phys.* **1976***, 64*, 1869-1876.

84. Baughman, R. H.; Change, R. R. *J. Polym. Sci., Polym. Phys. Ed.* **1976***, 14***,** 2019-2035.
85. Young, R. J.; Baughman, R. H. *J. Mater. Sci.* **1978,** *13*, 55-61.
86. Mawhinney, R. C.; Goddard, J. D. *Inorg. Chem.* **2003***, 42*, 6323-6337.
87. Besenyei, E.; Eigendorf, G. K.; Frost, D. C. *Inorg. Chem.* **1986***, 25*, 4404-4408.
88. Schettino, V.; Bini, R. *Phys. Chem. Chem. Phys.* **2003**, *5*, 1951-1965.
89. Hemley, R. J. *Annu. Rev. Phys. Chem.* **2000**, *51*, 763-800.
90. Bini, R.; Ceppatelli, M.; Citroni, M.; Schettino, V. *Chem. Phys.* **2012,** *398*, 262-268.
91. Cohen, M. D.; Schmidt, G. M. J. *J. Chem. Soc.* **1964***,* 1996-2000.
92. Ciabini, L.; Santoro, M.; Bini, R.; Schettino, V. *Phys. Rev. Lett.***2002***, 88*, 085505-4.
93. Ciabini, L.; Gorelli, F. A.; Santoro, M.; Bini, R.; Schettino, V.; Mezouar, M. *Phys. Rev. B.* **2005***, 72*, 094108-7.
94. Ciabini, L.; Santoro, M.; Gorelli, F. A.; Bini, R.; Schettino, V.; Raugei, S. *Nat. Mater.* **2007***, 6*, 39-43.
95. Sakashita, M.; Yamawaki, H.; Aoki, K. *J. Phys. Chem.* **1996**, *100*, 9943-9947.
96. Bernasconi, M.; Chiarotti, G. L.; Focher, P.; Parrinello, M.; Tosatti, E. *Phys. Rev. Lett.* **1997**, *78*, 2008-2011.
97. Dunn, K. J.; Bundy, F. P.; Interrante, L. V. *Phys. Rev. B* **1981**, *23*, 106-111.
98. Love, P.; Labes, M. M. *J. Chem. Phys.***1979,** *70*, 5147-5150.
99. Kelly, P. F.; Slawin, A. M. Z. *Angew. Chem. Int. Ed. Engl.* **1995***, 34*, 1758-1759.

100. Aucott, S. M.; Dale, S. H.; Elsegood, M. R. J.; Holmes, K. E.; James, S. L. M.; Kelly, P. F. *Acta Cryst.* **2004**, *C60,* m643-644.

101. Kelly, P. F.; Slawin, A. M. Z. *J. Chem. Soc., Dalton Trans.* **1996**, *21*, 4029-4030.

102. Aucott, S. M.; Drennan, D.; James, S. L. M.; Kelly, P. F.; Slawin, A. M. Z. *Chem. Commun.* **2007***, 29*, 3054-3056.

103. Maaninen, A.; Laitinen, R. S.; Chivers, T.; Pakkanen, T. A. *Inorg. Chem.* **1999***, 38*, 3450-3454.

104. Risto, M. Syntheses, Structures, and Bonding of Novel Chalcogen-Nitrogen Heterocycles. PhD. Dissertation, University of Oulu, Oulu, 2009.

105. Maaninen, T.; Chivers, T.; Laitinen, R.; Schatte, G.; Nissinen, M. *Inorg. Chem.* **2000***, 39*, 5341-5347.

106. Maaninen, T.; Laitinen, R.; Chivers, T. *Chem. Commun.* **2002***,* 1812-1813.

107. Gindl, J.; Björgvinsson, M.; Roesky, H. W.; Freire-Erdbrügger, C.; Sheldrick, G. M. *J. Chem. Soc. Dalton Trans.***1993***,* 811-812.

108. Risto, M.; Eironen, A.; Männistö, E.; Oilunkaniemi, R.; Laitinen, R. S.; Chivers, T. *Dalton Trans.* **2009**, 8473-8475.

109. Risto, M.; Konu, J.; Oilunkaniemi, R.; Laitinen, R. S.; Chivers, T. *Polyhedron* **2010***, 29*, 871-875.

110. Chivers, T.; Schatte, G. *Can. J. Chem.* **2003***, 81*, 1307-1314.

111. Chivers, T.; Parvez, M.; Schatte, G. *Angew. Chem. Int. Ed.* **1999***, 38*, 2217-2219.

112. Chivers, T.; Parvez, M.; Schatte, G. *Inorg. Chem.* **1999***, 38*, 5171-5177.

113. Pyykkö, P.; Runeberg, N.; Mendizabal, F. *Chem. Eur. J.* **1997***, 3*, 1451-1457.

114. Pyykkö, P. *Chem. Rev.* **1997***, 97*, 597-636.

115. Pyykkö, P. *Angew. Chem. Int. Ed. Engl.* **2004***, 43*, 4412-4456.

116. Hayet, S.; Hasan, S.; Mori, M.; Fariduddin, Q.; Ahmed, A. *Nitric Oxide in Plant Physiology*, Hayet, S.; Mori, M.; Pichtel, J.; Ahmed, A. Eds. Weinheim: Wiley-VCH, 2010; pp 1-3.

117. Andreev, R. V.; Borodkin, G. I.; Shubin, V. G. *Russ. J. Org. Chem.* **2013***, 49*, 432-438 and references cited therein.

118. Müller, B.; Poleschner, H.; Seppelt, K. *Dalton Trans.* **2008**, *33,* 4424-4427.

119. Itoh, T.; Tsutsumi, N.; Ohsawa, A. *Bioorg. Med. Chem. Lett.* **1999***, 9*, 2161-2166.

120. Tsutsumi, N.; Itoh, T.; Ohsawa, A. *Chem. Pharm. Bull.* **2000***, 48***,** 1524-1528 and references cited therein.

121. Tabellion, F. M.; Seidel, S. R.; Arif, A. M.; Stang, P. J. *J. Am. Chem. Soc.* **2001**, *123*, 7740-7741.

122. Marsden, C. J.; Smith, B. J. *J. Phys. Chem.* **1988**, *92*, 347-353.

123. Sacerdoti, M.; Gilli, G.; Domiano, P. *Acta Crystallogr.* **1975**, *B31*, 327-329.

124. Bartkowska, B.; Kruger, C. *Acta Crystallogr.* **1997***, C53*, 1064-1066.

125. Dierchks, H.; Krebs, B. *Angew. Chem. Int. Ed. Engl.* **1977***, 16*, 313-313.

126. Hürter. H. U.; Krebs, B. *Angew. Chem.* **1980***, 92*, 479-480.

127. Vinatier, P.; Gravereau, P.; Ménétrier, M.; Trut, L.; Levasseur, A. *Acta Crystallogr.* **1994***, C50*, 1180-1183.

128. Hiltmann, F.; Krebs, B. *Z. Anorg. Allg. Chem.* **1995**, *621*, 424-430.

129. Hiltmann, F.; Jansen, C.; Krebs, B. *Z. Anorg. Allg. Chem.* **1996**, *622*, 1508-1514.

130. Hammerschmidt, A.; Jansen, C.; Küper, J.; Köster, C.; Krebs B. *Z. Anorg. Allg. Chem.* **2001**, *627*, 669-674.

131. Hammerschmidt, A.; Köster, C.; Küper, J.; Lindemann, A.; Krebs, B. *Z. Anorg. Allg. Chem.* **2001**, *627*, 1253-1258.

132. Hammerschmidt, A.; Döch, M.; Wulff, M.; Krebs B. *Z. Anorg. Allg. Chem.* **2002**, *628*, 2637-2640.

133. Kuchinke, J.; Küper, J.; Krebs, B. *Z. Naturforsch., Teil B* **2002**, *57*, 1433-1438.

134. Krebs, B.; Hamann, W. *J. Less-Common Met.* **1988**, *137*, 143-54.

135. Geng, L.; Cheng, W. D.; Zhang, W. L.; Li, Y. U.; Luo, Z. Z.; Zhang, H.; Lin, C. S.; He, Z. Z. *Dalton trans.* **2011**, *40*, 4474-4479.

136. Geng, L.; Cheng, W. D.; Zhang, W. L.; Lin, C. S.; Zhang, H.; Li. Y. Y.; He, Z. Z. *Inorg. Chem.* **2010**, *49*, 6609-6615.

137. Hunger, J.; Borna, M.; Kniep, R. *J. Solid State Chem.* **2010**, *183*, 702-706.

138. Borna, M.; Hunger, J.; Kniep, R. *Z. Kristallogr. NCS* **2010***, 225*, 217-218.

139. Borna, M.; Hunger, J.; Kniep, R. *Z. Kristallogr. NCS* **2010***, 225*, 223-224.

140. Borna, M.; Hunger, J.; Kniep, R. *Z. Kristallogr. NCS* **2010***, 225*, 225-226**.**

141. Mock, M. T.; Potter, R. G.; Camaioni, D. M.; Li, J.; Dougherty, W. G.; Kassel, W. S.; Twamley, B.; BuBois, D. L. *J. Am. Chem. Soc.* **2009***, 131*, 14454-14465.

142. Kim, Y.; Martin, S. W. *Inorg. Chem.* **2004***, 43*, 2773-2775.

143. Borna, M.; Hunger, J.; Ormeci, A.; Zahn, D.; Burkhardt, U.; Carrillo-Cabrera, W.; Cardoso-Gil, R.; Kniep, R. *J. Solid State Chem.* **2011**, *184*, 296-303.
144. Hammerschmidt, A.; Lindemann, A.; Köster, C.; Krebs, B. *Z. Anorg. Allg. Chem.* **2001**, *627*, 2121-2126.
145. Hammerschmidt, A.; Lindemann, A.; Döch, M.; Krebs, B. *Z. Anorg. Allg. Chem.* **2003***, 629,* 1249-1255.
146. Hammerschmidt, A.; Döch, M.; Pütz, S.; Krebs, B. *Z. Anorg. Allg. Chem.* **2004**, *630*, 2299-2303.
147. Hammerschmidt, A.; Döch, M.; Pütz, S.; Krebs, B. *Anorg. Allg. Chem.* **2005***, 631*, 1125-1128.
148. Hammerschmidt, A.; Jansen, C.; Küper, J.; Püttmann, C.; Krebs, B. *Z. Anorg. Allg. Chem.* **1995**, *621*, 1330-7.
149. Jansen, C.; Küper, J.; Krebs, B. *Z. Anorg. Allg. Chem.* **1995**, *621,* 1322-9.
150. Püttmann, C.; Diercks, H.; Krebs, B. *Phosphorus, Sulfur, Silicon* **1992**, *65*, 1-4.
151. Chopin, F.; Hardy, A. *C. R. Acad. Sci.* **1965***, 261*, 142-4.
152. Chopin, F.; Turrell, G. *J. Mol. Struct.* **1969,** *3*, 57-65.
153. Inorganic Crystal Structure Database, version 2013/04; http://www.fiz-karlsruhe.de/icsd_home.html (accessed April 19, 2013).
154. Bergerhoff, G.; Brown, I.D. *Crystallographic Databases*, F.H. Allen et al. (Hrsg.) Chester, International Union of Crystallography, 1987.